Master's Thesis

Synthesis and characterization of size-controlled FeCo nanoparticles and composites with graphene

Sangmin Park

Department of Materials Science and Engineering

Graduate School of UNIST

2018

Synthesis and characterization of size-controlled FeCo nanoparticles and composites with graphene

Sangmin Park

Department of Materials Science and Engineering

Graduate School of UNIST

Synthesis and characterization of size-controlled FeCo nanoparticles and composites with graphene

A thesis
submitted to the Graduate School of UNIST
in partial fulfillment of the
requirements for the degree of
Master of Science

Sangmin Park

14. 12. 2017
Approved by

Advisor
Jae Sung Son

Synthesis and characterization of size-controlled FeCo nanoparticles and composites with graphene

Sangmin Park

This certifies that the thesis of Sangmin Park is approved.

12/14/2017 of submission

Advisor: Jae Sung Son

Wook Jo

Kwangjin An

Abstract

Synthesis and characterization of size-controlled FeCo nanoparticles and composites with graphene

Sangmin Park

School of Materials Science and Engineering

The Graduate School

Ulsan National Institute of Science and Technology

Nanoparticle usually refers to the particle which is ranging from one to one-hundred nm. They have unique properties which can't be seen in bulk materials; high surface to volume ratio, quantum size effect, surface plasmon resonance and so on. Among nanocrystals, magnetic nanoparticles are hot topics because of their wide usages for application such as catalysis, nano-medicine, electromagnetic wave absorption, bio-sensors and data storage. In the first part of the paper, I briefly introduced overall description of magnetic nanoparticles including magnetism, properties, synthetic method.

Iron cobalt(FeCo) nanoparticles are one of important magnetic nanoparticles because of their large values of permeability and saturation magnetization. So, they can be used in wide range of application. So, there have been many researches to synthesize FeCo nanoparticles. Nevertheless, synthesis of oxygen-free monodisperse FeCo nanoparticles remains challenging. In this paper, the new synthetic method synthesizing of FeCo nanoparticles is introduced. During synthesis, hydrogen gas was directly injected throughout the reaction time, leading to the reduction of oxygen part of the nanoparticles. I also synthesized size and shaped controlled FeCo nanoparticles by controlling the amount and ratio of oleic acid and oleylamine.

I also fabricated magnetic nanoparticles and edge-oxidized graphene (EOG) nanocomposites. Graphene has also attracted considerable attention from a number of different research areas, because it has great potential for a wide usages in application like catalyst, optoelectronic materials, sensors. There are many attempts to fabricate nanoparticles/graphene composites by EDC coupling, in-situ fabrication and so on. In this paper, I synthesized magnetic nanoparticles and EOG composite. EOG has carboxylic acid and hydroxyl functionalities only at the edge of it. So, it has great dispensability on water and better electrical properties than graphene oxide, expecting the superior properties to graphene oxide. I

synthesized the composite using two methods; One is EDC coupling and the other is using electrostatic interaction. In second method, the surface of FeCo nanoparticles are exchanged organic ligands into inorganic ligands to give the negative surface charge, while PEI-coated graphene oxide has positive charge. I fabricated FeCo nanoparticles and EOG hybrid materials through electrostatic interaction.

Contents

List of Figures

List of Tables

Chapter 1. Theoretical background of magnetic nanoparticles

1.1 Introduction

Nanoparticle usually refers to the particle which is ranging from 1 to 100 nm. They have unique properties which can't be seen in bulk materials; high surface to volume ratio, quantum size effect[1], magnetic properties[2], surface plasmon resonance[3] and so on. There are many scientific researches on nanoparticles, because nanoparticles have great potential of wide range of application such as biology, physics, optics and electronics[4-6]. Magnetic nanoparticle is one of the kind of nanoparticle. Magnetic nanoparticle also has unique magnetic properties including high magnetic susceptibility, single-domain effect, superparamagnetic and so on.[7] Magnetic nanoparticles have been a hot topic because they have potential using in various application including catalysis[8], nano-medicine[9], magnetic resonance imaging[10], data storage[11], electromagnetic wave absorption (Figure 1).[12] In this chapter, I first discuss the magnetism briefly. After that, special features of magnetic nanoparticles are introduced. Finally, methods of synthesizing magnetic nanoparticles are discussed.

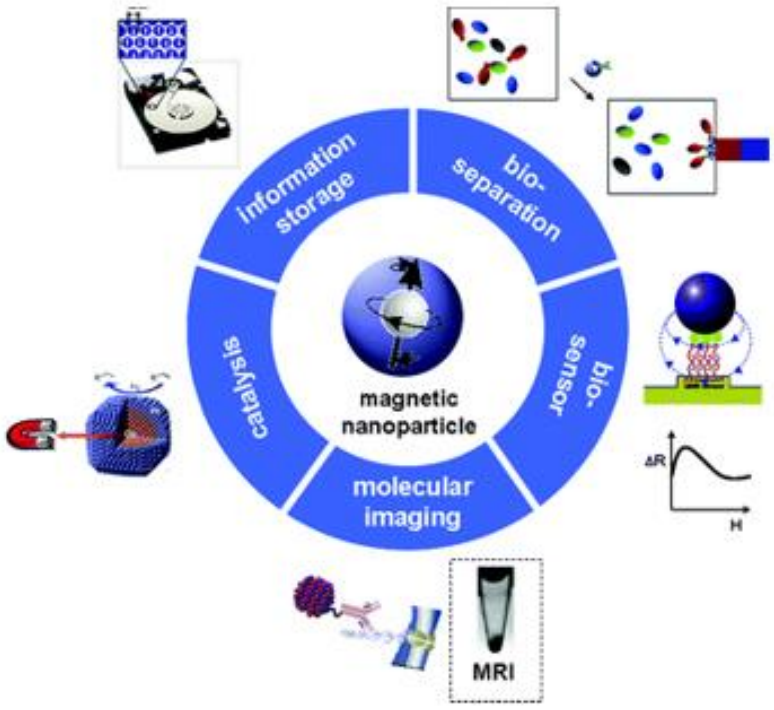

Fig. 1.1. The various applications of magnetic nanoparticles.

1.2 Magnetism

The behavior of magnetic nanoparticles under external magnetic field is determined by susceptibility and permeability. Susceptibility (χ) indicates the degree of materials are attracted into or repelled out under external magnetic field. In other words, susceptibility describes the relationship between the magnetization level (M) and the external magnetic field (H):

$$M = \chi H \quad (1.1)$$

Paramagnetic and ferromagnetic materials have positive susceptibility. On the contrary, if the susceptible is less than zero, the material is said to be diamagnetic. Permeability (μ) describes the relationship between the magnetic induction (B) induced by the external magnetic field (H):

$$B = \mu H \quad (1.2)$$

Materials can be divided into several groups divided by magnetic behaviors; diamagnetic, paramagnetic, ferromagnetic, antiferromagnetic, and ferrimagnetic. The overall characteristic of magnetic behaviors can be seen in Figure 1.2.[13]

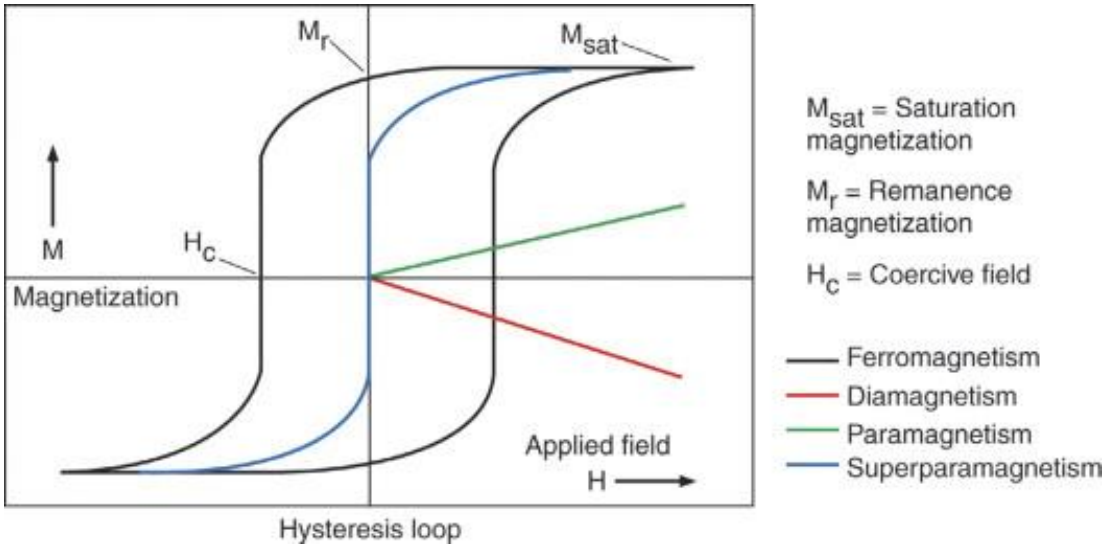

Fig. 1.2. Characteristic hysteresis loops and graphs of magnetization(M) versus applied magnetic field(H) of ferromagnetic, superparamagnetic, diamagnetic, paramagnetic. M_r indicates the remanence and H_c is coercivity. This figure is reproduced with permission from Ref. [13], Elsevier.

1.2.1 Diamagnetism

Under the external magnetic field, magnetic moment is induced antiparallel to the field in diamagnetic substances. So, they have tiny or negative susceptibility(χ). There are usually no unpaired electrons in

these materials, which can't produce intrinsic electron magnetic moments. Bismuth, antimony, indium, gold and most of organic compounds are examples of diamagnetic materials.[14]

1.2.2 Paramagnetism

Under the external magnetic field, there are magnetic forces induced parallel to the field in paramagnetic materials. They have small positivity susceptibility. There are unpaired electrons in paramagnetic materials. Owing to the unpaired electrons, there are intrinsic electron magnetic moments. But if the external field is eliminated, they do not have magnetic moments anymore. Aluminum, tin, platinum, oxygen are examples of paramagnetic materials.[15]

Paramagnetic material	χ	Diamagnetic material	χ
Aluminum	2.3 X 10^{-5}	Bismuth	- 1.66 X 10^{-5}
Calcium	1.9 X 10^{-5}	Copper	- 9.8 X 10^{-6}
Chromium	2.7 X 10^{-4}	Diamond	- 2.2 X 10^{-5}
Lithium	2.1 X 10^{-5}	Gold	- 3.6 X 10^{-5}
Magnesium	1.2 X 10^{-5}	Lead	- 1.7 X 10^{-5}
Niobium	2.6 X 10^{-4}	Mercury	- 2.9 X 10^{-5}
Oxygen	2.1 X 10^{-6}	Nitrogen	- 5.0 X 10^{-9}
Platinum	2.9 X 10^{-4}	Silver	- 2.6 X 10^{-5}
Tungsten	6.8 X 10^{-5}	Silicon	- 4.2 X 10^{-6}

Table 1.1. Magnetic susceptibilities of several paramagnetic and diamagnetic material at 300K.

1.2.3 Ferromagnetism

Ferromagnetic material has high and positive susceptibility. Although the magnetic field isn't applied into the substance, there are magnetic moments in ferromagnetic materials[16]. Permanent magnetic properties in these material is originated from atomic magnetic moments and orbital magnetic moment[17]. These materials have saturation magnetization (M_s), the maximum possible magnetization. The saturation magnetization is equal to sum of magnetic moment for each atom. If the temperature of material the increases, thermal motion and ferromagnetic tendency for dipoles have competed each other. When the temperature reaches at a certain point, the material has no a spontaneous magnetization, becoming paramagnetic materials. The point of temperature is referred to Curie temperature (T_c).[17] Fe, NiCo, and their alloys are examples of ferromagnetic materials.[18]

1.2.4 Antiferromagnetism

The spins of antiferromagnetic materials are aligned to magnetic field like ferromagnetic materials. But spins of adjacent atom have opposite direction. Consequently, the total magnetic moment is zero. MnO, CoO, NiO are examples of antiferromagnetic materials.[19]

1.2.5 Ferrimagnetism

Ferrimagnetic material has magnetic properties without magnetic field like ferromagnetic material. But adjacent electron spin pairs tend to point in reverse directions like antiferromagnetic materials. However, the net magnetic is not zero because of incomplete cancellation of spin moments. Most ferrites are examples of ferrimagnetic materials.[20] Figure 1.3 represents schematic electron spins behavior in a 1D crystal.

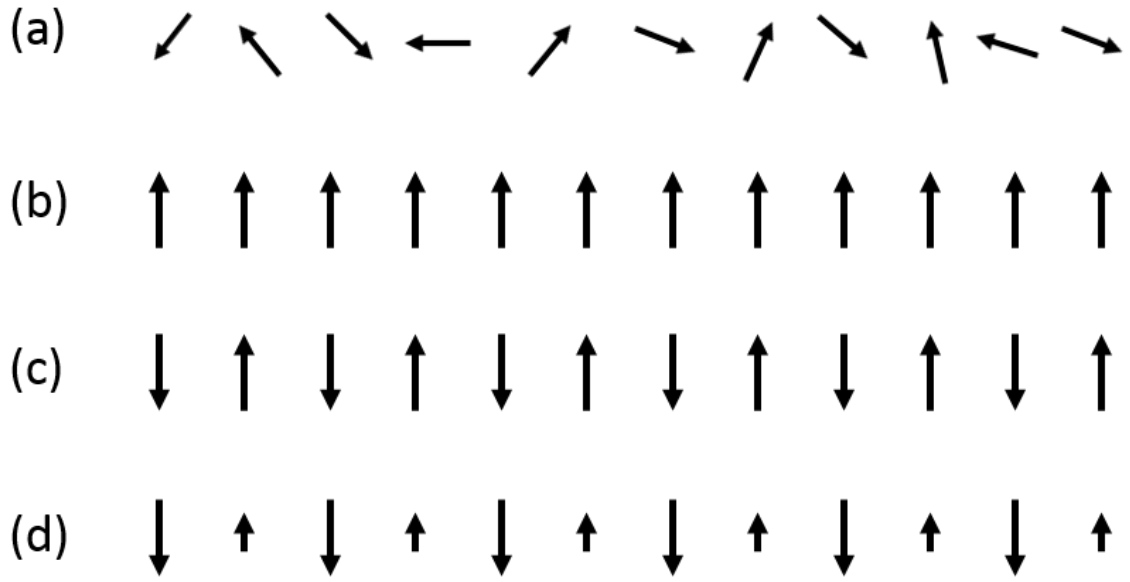

Fig. 1.3. Behaviors of electron spins in one-dimension; (a) paramagnetic; (b) ferromagnetic; (c) antiferromagnetic; (d) ferrimagnetic materials.

1.3 Properties of magnetic nanoparticles

There are many issues dominating the properties of magnetic nanoparticles. One of the most important factor is size of nanoparticles. Beside the size, surface morphology, composition and structure can change the magnetic properties of nanoparticles as well. In this part, special features of magnetic

nanoparticles are briefly introduced.

1.3.1 Size Effect

There are two special issues related to size of nanoparticles. One is single-domain effect and the other is superparamagnetic. In bulk magnetic materials, they have several domains to form structure. It means that the area of the material is divided by several domain walls. When size of magnetic nanoparticles is reached at a certain critical point, spins of free electron within the nanoparticles are aligned into one direction and the nanoparticles have a single-domain structure. The critical diameter (D_c) can be determined by the equation.

$$D_c \approx \frac{36\sqrt{AK}}{\mu_0 M_s^2} \quad (1.3)$$

A is the exchange constant, K is the effective anisotropy constant, μ_0 is the vacuum permeability, and M_s is the saturation magnetization. The value of D_c is usually between tens to hundreds of nanometers. The typical values of M_s, K, and D_c values of magnetic substances are summarized below table.[21]

Materials	M_s (emu cm^{-3})	K (10^6 J m^{-3})	D_c (nm)
Fe	1745	0.048	15
Co	1400	0.45	70
Ni	490	-0.005	55
Fe_3O_4	460	-0.011	128
$L1_0$-FePt	1140	7	60
$SmCo_5$	910	20	750

Table 1.2. The values of M_s, K, D_c of several typical magnetic materials

In case of a multi-domain nanoparticles, the magnetic moment arrangement directions are affected by several factors. One is anisotropy energy which can be explained by KV (V is the domain volume) and domain wall motion. But there is no domain wall motion in single-domain nanoparticles, so alignment of magnetization direction is only affected by KV. So, the single domain nanoparticles have higher coercivity than the multi-domain nanoparticles. The size-dependent coercivity values of ferromagnetic nanoparticles are shown in Figure 1.4.[22]

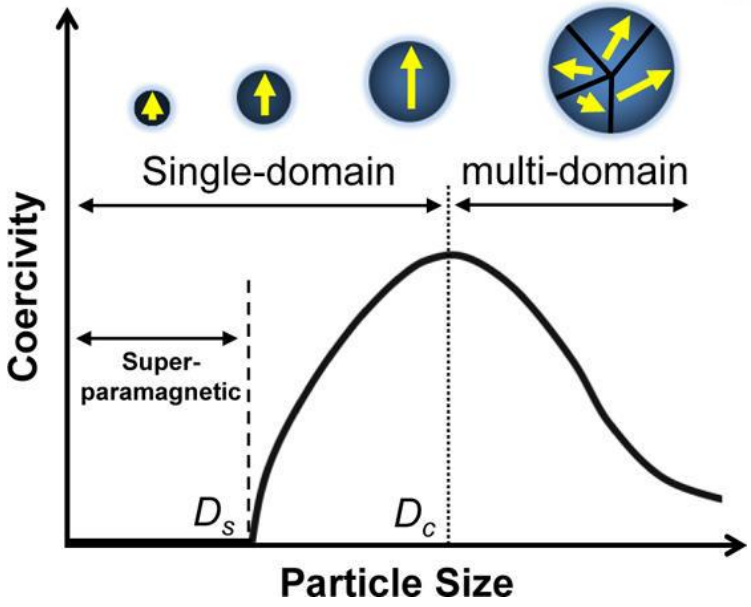

Fig. 1.4. Illustration of size-dependent H_c of a ferromagnetic particle. This figure is reproduced with permission from Ref. [22], ACS.

If the size of the nanoparticle continues to decrease, the nanoparticle becomes superparamagnetic material. As the nanoparticle size decrease, thermal energy k_bT (k_b : Boltzmann constant) and anisotropy energy KV compete each other, reducing coercivity. After size of nanoparticles reaching to a critical value D_s, which is called superparamagnetic limit, thermal energy overtakes anisotropy energy. In this state, the substance acts as a paramagnetic material, which means that the coercivity becomes zero. But it has larger saturation magnetization and susceptibility value than the paramagnet. Owing to the special properties, superparamagnetic materials have a good colloidal stability and are useful for biomedical applications. As their size is small, the surface effects become more important because of increasing the surface to volume ratios.

The saturation magnetization (M_s) of the magnetic nanoparticle is also affected by size. If the size of the magnetic nanoparticles is smaller, the M_s of the maganetic particle is also reduced because of spin-canting effect. The phenomenon is caused by spins are slightly tilted with respect to the axis, not parallel. The surfactant binding with a surface of nanoparticle quenches the spins of surface, so it reduces the saturation magnetization.

1.3.2 Shape and structure effect

Shape and structure are also important factor to determine magnetic properties. The estimation of critical diameter can be applied to spherical nanoparticles. Nanoparticles with high anisotropy have higher D_c and coercivity than spherical particles. For example, coercivity of iron nanoparticles becomes

more than 10 times when the aspect ratio becomes larger. The aspect ratio versus coercivity of iron nanoparticle is listed in Table 1.3.[23,24]

Aspect ratio	H_c [Oe]
1.1	820
1.5	3300
2.0	5200
5.0	9000
10	10100

Table 1.3. The coercivity of iron nanoparticles varying aspect ratio

Shape-dependent magnetic properties cobalt nanoparticles also have been experimentally demonstrated with several aspect ratios. In case of 15 nm sized cobalt nanorod with the aspect ratio of 10, the coercivity of the nanorod has 4500 Oe at room temperature.[25]

Structure of nanoparticle is also important factor to determine magnetic properties, because crystal structure affects intrinsic spin-orbital interaction. Figure 1.5 shows the two types of FePt alloy systems.[26,27] One of type is face centered cubic structure (fcc), referred to as A1 structure. The A1 structure is magnetically isotropic and soft. The other type is $L1_0$ structure, which is the face centered tetragonal (fct) structure. In this structure, iron and platinum atoms are forming the alternate stacking along the [001] direction. The fct structure is magnetically anisotropy due to the strong 3d (Fe) and 5d (Pt) coupling. Comparing each other, 10 nm of A1 FePt nanoparticles are superparamagnetic. But 10 nm of $L1_0$ FePt nanoparticles are strongly ferromagnetic materials. Cobalt nanoparticles also show the structure dependent magnetic properties. The fcc structure cobalt nanoparticles have smaller effective anisotropy constant (K) than hcp structure cobalt nanoparticles.[28]

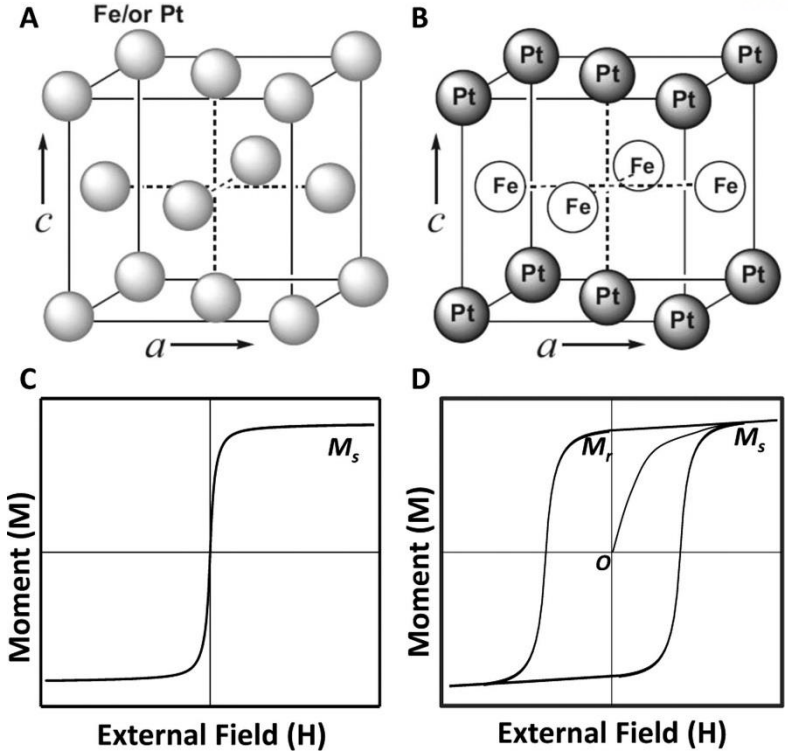

Fig. 1.5. (A and B) Schematics of the local structures of (A) A1-FePt and (B) $L1_0$-FePt. (C and D) Magnetic hysteresis loops of (C) superparamagnetic and (D) Ferromagnetic nanoparticles. This figure is reproduced with permission from Ref. [22], ACS.

1.3.3 Surface effect

As the size of nanoparticle become smaller, surface and interface affect the properties of nanoparticles, because most atoms are located at surface. In case of 1.6 nm fcc cobalt, for example, about 60 % of spins are positioned at the exterior region of nanoparticles. Because of the ratio of surface to volume, the exterior spins are important factor which can tune the magnetic properties. As the particles size decreases, the magnetization of the particle decreases due to surface effects, comparing with the bulk one. There are many possible reason such as the magnetically insulating layer on the surface, spin-canted, a spin glass like behavior of the surface spins. But there are also exceptions for some cases. In case of cobalt nanoparticles, for example, the magnetic moment increases as particle size decreases. Magnetic anisotropy (K_{eff}) is also affected by particle size.[29,30] K_{eff} can be described by the equation:

$$K_{eff} = K_v + \frac{6}{D}K_s \quad (1.4)$$

Where K_v is the bulk anisotropy energy constant, and K_s is the surface anisotropy energy constant. When the surface of the nanoparticle is modified such as absorbing different molecule, the value of K_{eff} changes. This is the reason why the surface anisotropy is important factor to K_{eff}.

There are also many efforts to change the magnetic properties of nanoparticles through coating the

nanoparticles. For example, if cobalt nanoparticle is coated to gold, then the degree of magnetic anisotropy become lower than uncoated cobalt nanoparticles.

1.3.4 Composition effect

Magnetic properties of MNPs are also affected by compositions. Oxygen anions of Fe_3O_4 forms close-packed fcc structure. Iron ions are located at octahedral (O) and tetrahedral sites (T). Fe_3O_4 can be described as $[Fe^{3+}]_T[Fe^{2+}Fe^{3+}]_OO_4$. Figure 1.6. shows the structure of Fe_3O_4.

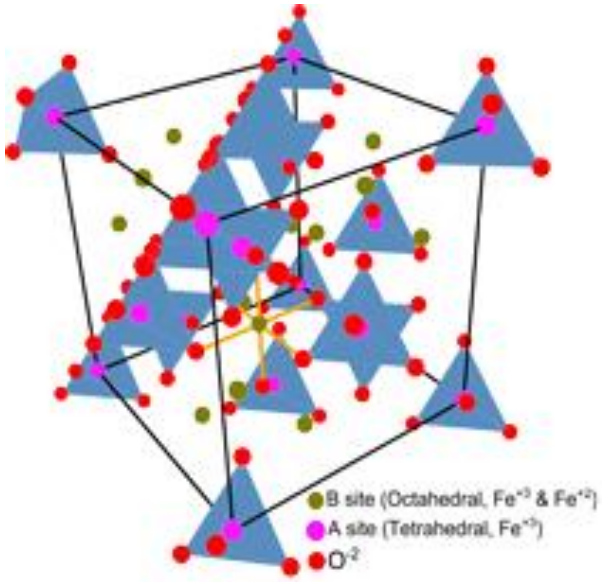

Fig. 1.6. Fe_3O_4 crystal structure with the pace group of Fd3m cubic lattice

Fe^{3+} of O and T sites cancel the magnetic moments. So, the net magnetic force of the Fe_3O_4 comes from the magnetic moments of Fe^{2+}. The net magnetization of the nanoparticle can be tuned by substituting Fe^{2+} with Mn^{2+}, Co^{2+} or Ni^{2+}. In case of 12 nm $MnFe_2O_4$, Fe_3O_4, $CoFe_2O_4$, and $NiFe_2O_4$, the saturation moments are 110, 101, 99 and 85 emu g^{-1},[31] respectively. The composition can also affect the coercivity. In case of FePt, for example, the coercivity is affected by the atomic ratio of Fe/Pt. The coercivity of Fe_xPt_{1-x} is largest when x = 0.55.[32,33]

1.4 The synthesis of magnetic nanoparticles

1.4.1 Overview

Controlling the particle's size, morphology, composition is important to use magnetic nanoparticles for the applications such as biomedicine, data storage, because various properties of the nanoparticles depend on the parameters. To synthesize monodisperse nanoparticle "burst-nucleation" concept is adopted. The concept suggests that it is important that nucleation occurs simultaneously, and additional nucleation should be prevented during the reaction. The method is also known as "the separation of nucleation and growth". The model which describes the burst nucleation concept is shown in Figure 1.7.[34]

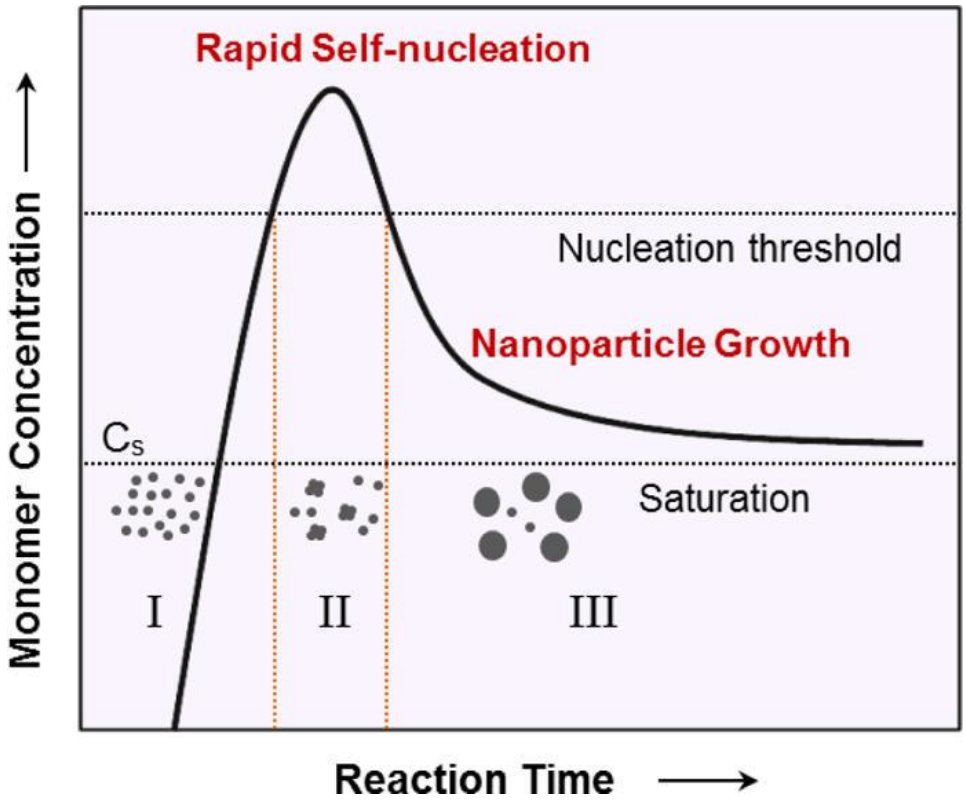

Fig. 1.7. LaMer model of synthetic process including nucleation and growth to monodisperse nanoparticles. This figure is reproduced with permission from Ref. [34], ACS.

In stage I, the precursors exist as "monomer". No precipitation occurs in stage I since energy barrier noted as "nucleation threshold" is large.[35] When the concentration of monomers reached at nucleation threshold (stage II), nuclei are formed. In other words, supersaturation degree is large so as to exceed the nucleation threshold for nucleation. As a result, monomer concentration is rapidly decreased. When

the monomer concentration reached at nucleation threshold, there aren't additional nuclei (stage III). The section is referred as to growth stage. In this stage, the additional nucleation is prevented, and the growth of nanoparticles continues until reaction solution is supersaturated.

1.4.2 Thermal decomposition

There are several methods to achieve the "burst nucleation" concept. One method is "hot-injection" method. At a high temperature, the rapid injection of reaction precursors can result in the burst nucleation of nanoparticles, followed by controlling growth to form monodisperse nanoparticles. "Hot-injection" method is illustrated in Figure 1.8.[36]

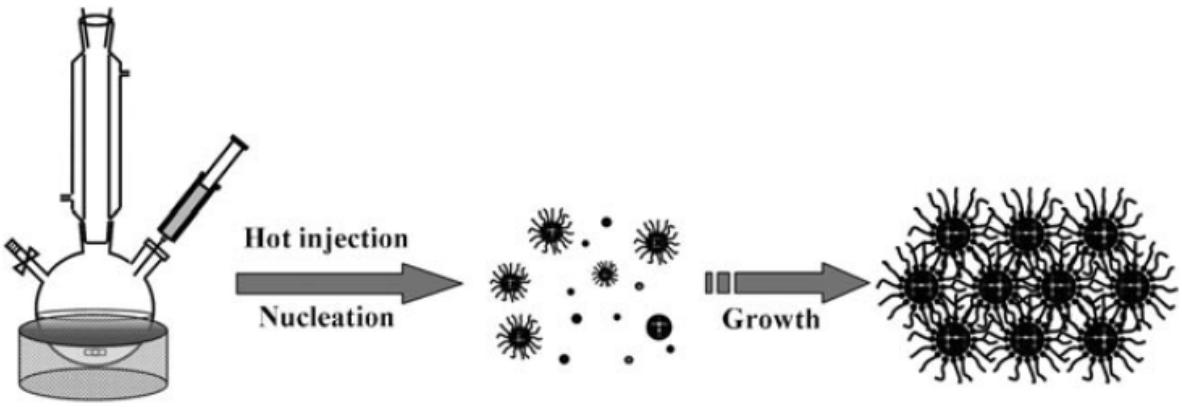

Fig. 1.8. "Hot-injection" synthesis of monodisperse nanoparticles. This figure is reproduced with permission from Ref. [34], ACS.

Many magnetic nanoparticles such as monodisperse Fe[37,38], Co[39,40] and Ni[41] nanoparticles can be synthesized through the method.[42,43] Another method is referred to as "heating-up" method. In this method, the mixture of precursors, surfactant, and solvent was added to the flask at 25°C and the reaction solvent is heated to a certain temperature to control nucleation and growth stage. Because of its simplicity, the method is used for the large-scale synthesis as it does not require the rapid injection of a large amount of reactant solution into the reaction mixture. J. Park et al. used the heating up method to synthesize large-scale size uniformed Fe_3O_4 nanoparticles. They used $FeCl_3$ which is not toxic and expensive as precursor and sodium oleate which can react with precursors and form an iron oleate complex as a surfactant. The metal-oleate complex is decomposed at 240 and 320°C in various solvent like octyl ether, 1-octadecene or 1-hexadecene. The Fe_3O_4 size are ranging from 5 to 22 nm, varying the experimental conditions like reaction time and temperature. Overall process is described in Figure 1.9.[43]

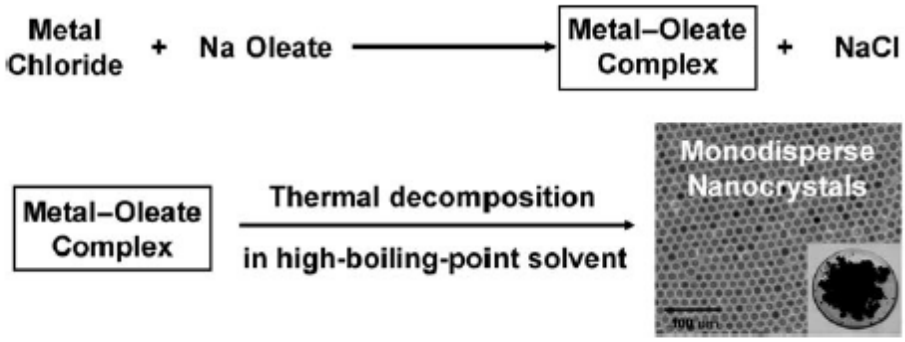

Fig. 1.9. Scheme of synthesis of large-scale uniform sized iron oxide nanoparticles. Metal chlorides are reacted with sodium oleate, leading to from metal-oleate complex. Metal oleate precursors have high boiling point and decomposition of the precursors produces monodisperse nanoparticles. This figure is reproduced with permission from Ref. [43], Nature Publishing Group.

Thermal decomposition method is widely used because of many advantages, including nanoparticles synthesized with the method have uniform size and high crystallinity. Also, they have dispersity in organic solvents.

1.4.3 Co-precipitation

Co-precipitation is the precipitation of a normally soluble component from the solution. With this method, nanoparticle can be synthesized simply and conveniently. Co-precipitation is based on the chemical reactions carried out in a mono-phase liquid medium, and it allows nucleation and growth to be controlled. Although the method is easy and can be conducted in ambient condition, there are several disadvantages compared to thermal decomposition method. They are usually polydisperse and have low crystallinity. To synthesis iron oxide nanoparticles, mixture of FeO(OH) and a base such as ammonium hydroxide or sodium hydroxide are added to a solution iron salts (figure 1.10).[44,45]

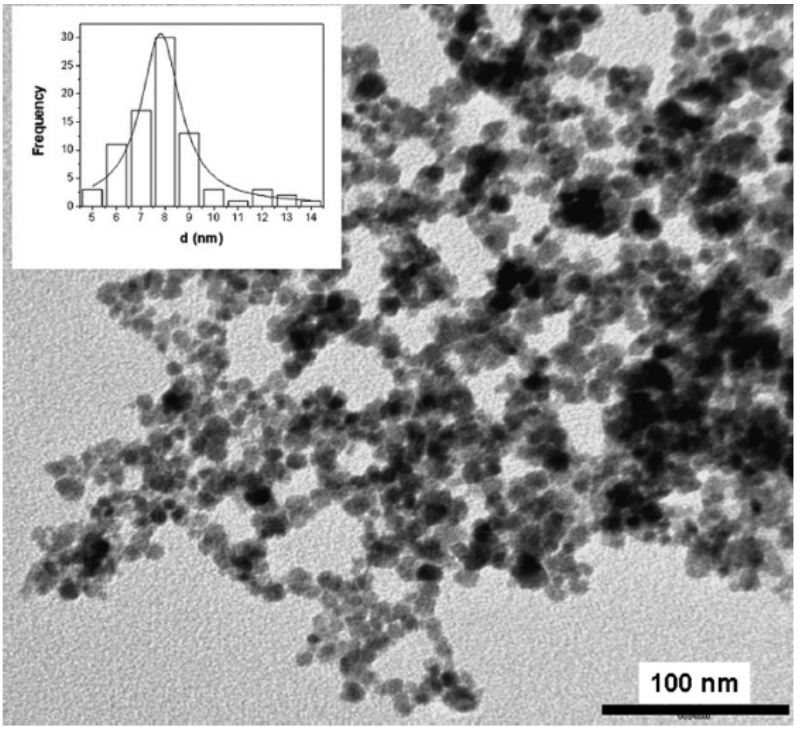

Fig. 1.10. TEM images of nanometer Fe_3O_4 particles synthesized with coprecipitation method. Size histogram of the nanoparticle on the left top of the picture. This figure is reproduced with permission from Ref. [45], Elsevier.

Then, the precipitate can be separated by magnetic separation or centrifugation. The result product is treated by base or acid solution to stabilize the resultant. The reaction equation is described below.

$$Fe^{2+} + 2Fe^{3+} + 8OH^- \rightarrow Fe_3O_4 + 4H_2O \quad (1.5)$$

If the resultant is heated with the surfactant such oleic acid, the precipitates are sterically stabilized. The geometry and magnetic properties of nanoparticles can be tuned by varying the experimental factors like temperature, salt, injection fluxes, presence of oxygen, ion strength and pH and so on.[46]

1.4.4 Hydrothermal synthesis

The hydrothermal synthesis is techniques performed at high temperature (> 200°C) and high pressure (> 13,790 kPa) using autoclaves or reactors.[47,48] A broad range of nanoparticles can be formed under hydrothermal conditions. High temperature makes the nucleus and growth of the nanoparticles more rapidly. As a result, small sized nanoparticles are formed. In this method, morphologies such as size and shape of the nanoparticle can be tuned with the parameter like the temperature, the reaction time, the concentration of reactant, solvent, precursors, and so on.

1.4.5 Microemulsion

Microemulsion are isotropic liquid mixture of oil, water and surfactant, but thermodynamically stable. The phase exists as microdroplets which sizes vary 1 to 50 nm, forming reverse micelle. The micelle sizes can be controlled by controlling the ratio of their compositions.[49] If the desired reactants are added to the water-in-oil micro emulsions, a precipitation forms in the micelles. Then, the resultant can be separated by magnetic separation or centrifugation. With reverse micelles of cetyltrimethylammonium bromide, using 1-butanol as cosurfactant and octane as the oil phase, various nanoparticles such as metallic cobalt, cobalt/platinum alloys can be synthesized. $MnFe_2O_4$ nanoparticles with the size can be fabricated with the formation of water-toluene reverse micelles with NaDBS surfactant (Figure 1.11). A NaDBS solution is added to the mixture of $Mn(NO_3)_2$ and $Fe(NO_3)_3$. After that, toluene is added to the reactant to form reverse micelles. So the size of the $MnFe_2O_4$ nanoparticles can be controlled by controlling the ratio of water and toluene.[50]

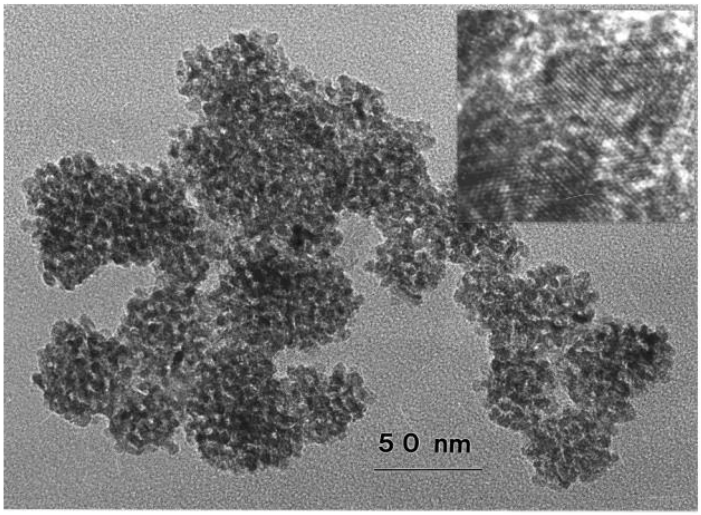

Fig. 1.11. TEM images of $MnFe_2O_4$ nanoparticles synthesized with microemulsion method. This figure is reproduced with permission from Ref. [45], ACS.

Besides these techniques which are referred above, there are many methods to synthesize magnetic nanoparticles, including electron beam lithography, gas-phase deposition, sol-gel method, flow injection method and so on. Magnetic nanoparticles synthesized with thermal decomposition methods have best quality among above methods. Because they have monodispersivity and are easy to control morphology like size and shape of the magnetic nanoparticles. Summary of the synthesis strategy are shown below table.[51]

Synthetic method	Synthesis	Reaction temp. [°C]	Reaction period	Solvent	Surface-capping agents	Size distribution	Shape control	Yield
co-precipitation	very simple, ambient conditions	20–90	minutes	water	needed, added during or after reaction	relatively narrow	not good	high/ scalable
thermal decomposition	complicated, inert atmosphere	100–320	hours–days	organic compound	needed, added during reaction	very narrow	very good	high/ scalable
microemulsion	complicated, ambient conditions	20–50	hours	organic compound	needed, added during reaction	relatively narrow	good	low
hydrothermal synthesis	simple, high pressure	220	hours ca. days	water-ethanol	needed, added during reaction	very narrow	very good	medium

Table 1.4. Comparison of co-precipitation, thermal decomposition, mircoemulsion, hydrothermal methods.

Chapter 2. The synthesis of size- and shape-controlled FeCo nanoparticles

2.1 Introduction

FeCo nanoparticles are attracting great attention soft ferromagnetic materials. Because they have great magnetic properties including large value of saturation magnetization and permeability. Because of their magnetic properties, FeCo nanoparticles are widely used in various application such as magnetic storage, bio-sensor, magnetic resonance imaging and electromagnetic-wave absorption.[53-56] So, there have been many attempts to synthesize FeCo nanoparticle alloys owing to their industrial importance. D.Kodama et al.[57] reported that they synthesized 35-200 nm FeCo nanoparticles using polyol process with $FeCl_2 \cdot 4H_2O$, $Co(acetate)_2 \cdot 4H_2O$ NaOH and PVP. And Chaubey et al.[58] introduced a route to synthesize 10 – 20 nm FeCo nanoparticles based on thermal decomposition using $Fe(acac)_3$, $Co(acac)_2$, 1,2-hexadecanediol, oleic acid and oleylamine with flowing gas mixture of argon and hydrogen. A fraction of hydrogen protects the FeCo nanoparticles from oxidation. In addition, Shin et al.[59] synthesized FeCo nanoparticles by coprecipitation route and Guo et al.[60] synthesized FeCo, Fe, Co nanoparticles with wet chemistry.

In this paper, I synthesized low oxygen containing FeCo nanoparticles and control the shape and size of the nanoparticles. Through direct hydrogen gas injection into reaction mixture, cobalt ferrites are reduced to iron cobalt. Also, I synthesized various morphology of FeCo nanoparticles with adjusting the amount and ratio of surfactant.

2.2 Experimental method

Chemicals

Iron (III) acetylacetonate ($Fe(acac)_3$, 99.9 %, Sigma-Aldrich), cobalt (II) acetylacetonate ($Co(acac)_2$, 97 %, Sigma-Aldrich), 1,2-hexadecanediol (90 %, Sigma-Aldrich), oleic acid (OA, 90 %, Sigma-Aldrich), oleylamine (Olam, 70 %, Sigma-Aldrich), 1-octadecene (ODE, 90 %, Sigma-Aldrich)

Characterization

Transmission electron microscopy (TEM) images of nanocrystals (NCs) were obtained using a JEOL-2100 instrument operated at 200 kV. X-ray diffraction (XRD) patterns were collected using a Rigaku D/Max-3C diffractometer equipped with a rotating anode and a Cu Kα radiation source.

Synthesis of 20 nm FeCo nanoparticles,

All reactions were performed with Schlenk line technique. At first, $Fe(acac)_3$ (0.265 g, 0.75 mmol), $Co(acac)_2$ (0.129 g, 0.5 mmol), 1,2-hexadecandiol (0.387 g, 1.5 mmol), OA (6.4 mL, 20 mmol) and Olam (3.4 mL, 10 mmol) were added to a 50 mL flask. Using a needle, H_2 7% + Ar 93% gas mixture was directed injected into the reaction solvent. And the mixture was degassed for twenty minutes using H_2 7% + Ar 93% gas. The temperature of mixture was raised to 100ºC and maintain the temperature for 10 minutes. Then, the temperature of mixture was raised to 300ºC and refluxed for 2 hours. After cooling it to 25ºC, 5 mL of hexane was injected in the reaction mixture. The synthesized FeCo nanoparticles were precipitated by the addition of 15 mL of ethanol and centrifugation (6000 rpm, 5 minutes) and re-dispersed in hexane. The washing process were done several times to remove the residual of the resultant. Final product was dispersed in 10 mL of hexane.

Synthesis of 13 nm FeCo nanoparticles

$Fe(acac)_3$ (0.265 g, 0.75 mmol), $Co(acac)_2$ (0.129 g, 0.5 mmol), 1,2-hexadecandiol (0.387 g, 1.5 mmol), OA (4.8 mL, 15 mmol) and Olam (5.1 mL, 15 mmol) were mixed in a 50 mL flask. The next procedures of the experiment are identical to above conditions.

Synthesis of 5 nm FeCo nanoparticles

$Fe(acac)_3$ (0.265 g, 0.75 mmol), $Co(acac)_2$ (0.129 g, 0.5 mmol), 1,2-hexadecandiol (0.387 g, 1.5 mmol), OA (1.07 mL, 3.33 mmol), Olam (2.27 mL, 6.67 mmol) and 10 mL of ODE were mixed in a 50 mL flask. The next procedures of the experiment are identical to above conditions.

Synthesis of star-shaped FeCo nanoparticles

$Fe(acac)_3$ (0.265 g, 0.75 mmol), $Co(acac)_2$ (0.129 g, 0.5 mmol), 1,2-hexadecandiol (0.387 g, 1.5 mmol), OA (7.68 mL, 24 mmol) and Olam (2.04 mL, 6 mmol) were mixed in a 50 mL flask. The next procedures of the experiment are identical to above conditions.

2.3 Result and discussion

2.3.1 Reduction of FeCo with hydrogen gas

I synthesized FeCo nanoparticles by thermal composition method with organometallic precursors under hydrogen atmosphere. Fe(III) acetylacetonate ($Fe(acac)_3$) and Co(II) acetylacetonate ($Co(acac)_2$) are

used as precursors, 1,2-hexadecanediol (HDD) as a reducing agent, and oleic acid(OA) and oleylamine(Olam) as a surfactant. There are several reports about the role of hydrogen in preventing FeCo nanoparticles from oxidation. Chaubey et al.[58] synthesized 10 – 20 nm monodisperse FeCo nanoparticles. They used a 7 % H_2 + 93 % Ar gas mixture for the reduction of oxygen. They check the reduction of oxygen by X-ray diffraction patterns. Poudyal et al.[61] also synthesis various size of FeCo nanoparticle using hydrogen gas. At first, they synthesis cobalt ferrite($CoFe_2O_4$) nanoparticles. The synthesized cobalt ferrite nanoparticles and sodium chloride powders were mixed, and annealed to 500°C in 7 % H_2 + 93 % Ar gas mixture. Sodium chloride made a matrix around the nanoparticles. It prevents the nanoparticles from agglomeration during annealing.

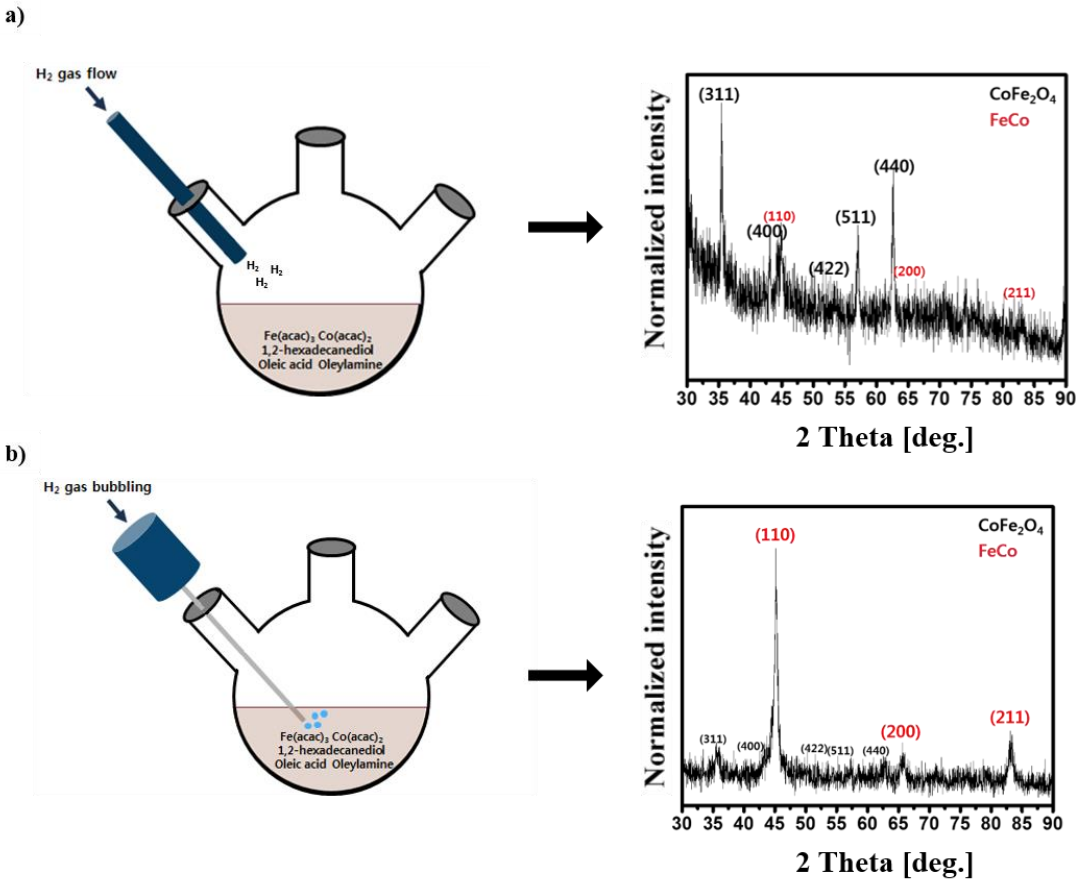

Fig. 2.1. Schematically illustrated procedure of synthesis of FeCo nanoparticles with hydrogen gas a) flowing and b) directly injected into reaction mixture, and their X-ray diffraction patterns.

For the further research, I directly injected the hydrogen gas into the reaction mixture during the synthesis procedure. For the comparison, I also synthesized FeCo nanoparticles with H_2 gas flowing, not bubbling. The scheme and result of the experiment are illustrated in figure 2.1. We checked as-synthesized FeCo nanoparticles by the method of hydrogen gas flow contained not a few oxygen

fractions, as can be seen X-ray diffraction pattern (Figure. 2.1a). On the contrary, FeCo nanoparticles by the method of direct hydrogen gas injection contained low-level of oxygen fractions, which means that hydrogen gas reduces the oxygen fractions of FeCo nanoparticles. (Figure. 2.1b) We also checked changes varying the amount of hydrogen gas. In a typical synthesis, a gas mixture (Ar 93 % + H_2 7 %) was injected with a flow rate 500 mL/minute. As the flow rate cutting in half, the peaks of $CoFe_2O_4$ fraction can be observed, implying that the lack of hydrogen gas (Figure 2.2a). I also synthesized FeCo nanoparticles with different solvent such as 1-octadecene and phenyl ether. In case of 1-octadecene, FeCo nanoparticles were well synthesized. But, in case of phenyl ether, there were no sign of FeCo(figure 2.2b), but $CoFe_2O_4$ however hydrogen gas injected. This phenomenon results from ether group (R-O-R') in phenyl ether. Oxygen from ether group prevent the formation of FeCo.

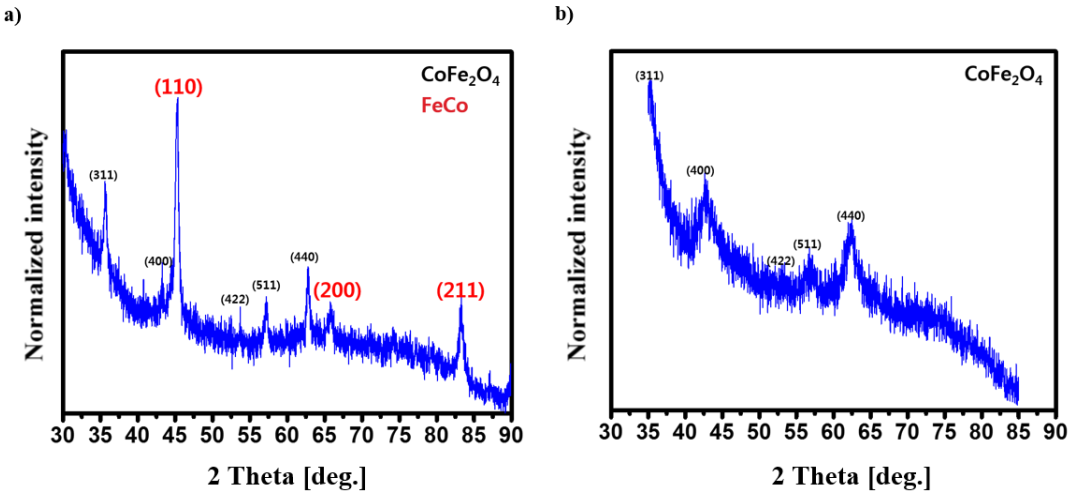

Fig. 2.2. X-ray patterns of as-synthesized magnetic nanoparticles: a) hydrogen gas directly injected into reaction mixture with the low flow rate b) using phenyl ether as a solvent

2.3.2 Synthesis of various size and shape of FeCo nanoparticles

In synthesis of iron cobalt nanoparitcles, I used oleic acid (OA) and oleylamine (Olam) as surfactants. The carboxylic group (-COOH) on OA and amine group (-NH_2) on oleylamine have different strength and selective binding energy with the surfaces of the nanoparticles.[62-65] OA is known to selectively and strongly bond to the crystalline facets such as a (100) plane. And Olam binds to the nanoparticles weakly and isotropically. Iron acetylacetonate and cobalt acetylacetone are decomposed at around 190°C. But they are reacted with oleic acid, resulting in metal oleates. So, the decomposition temperature is increased to 300°C. With the high temperature, the further growth can be done during synthesis

procedure.

I synthesized 13 and 20 nm FeCo nanoparticles varying the ratio of OA and Olam. With the fixed total amount of surfactants fixed to 30 mmol, I synthesized FeCo nanoparticles with several conditions: i) OA : Olam = 2 : 1, ii) OA : Olam = 1:1, iii) OA : Olam = 4 : 1. With the ratio of OA : Olam = 2 : 1, 20 nm FeCo nanoparticles were synthesized (Fig 2.3).

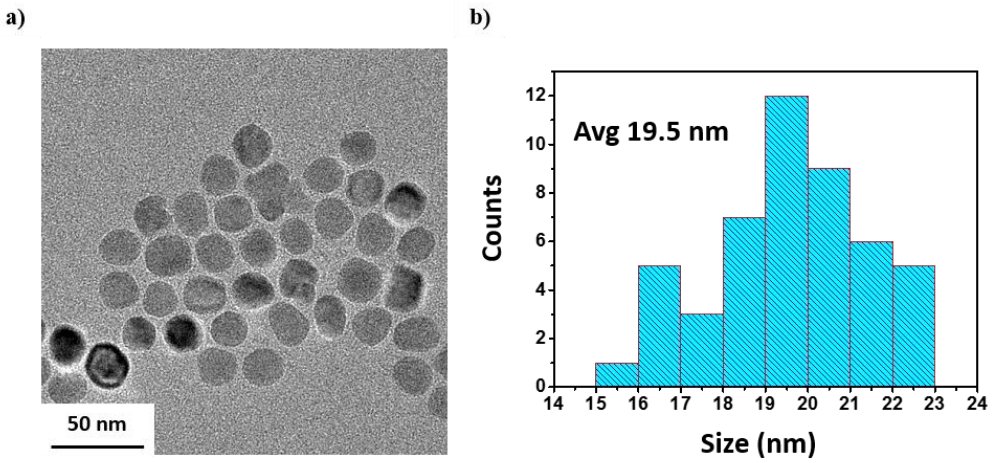

Fig. 2.3. a) TEM image and b) its size histogram of the as-synthesized 20 nm sized FeCo nanoparticles.

On the other hand, 13 nm FeCo nanoparticles are synthesized with the ratio of OA : Olam = 1 : 1 (Figure 2.4). In the presence of low oleic acid concentration, iron and cobalt acetylacetonate are quickly decomposed at low temperature. As a result, many small nuclei are formed during reaction and reduced iron and cobalt sources to feed the growth stage of nanoparticles.

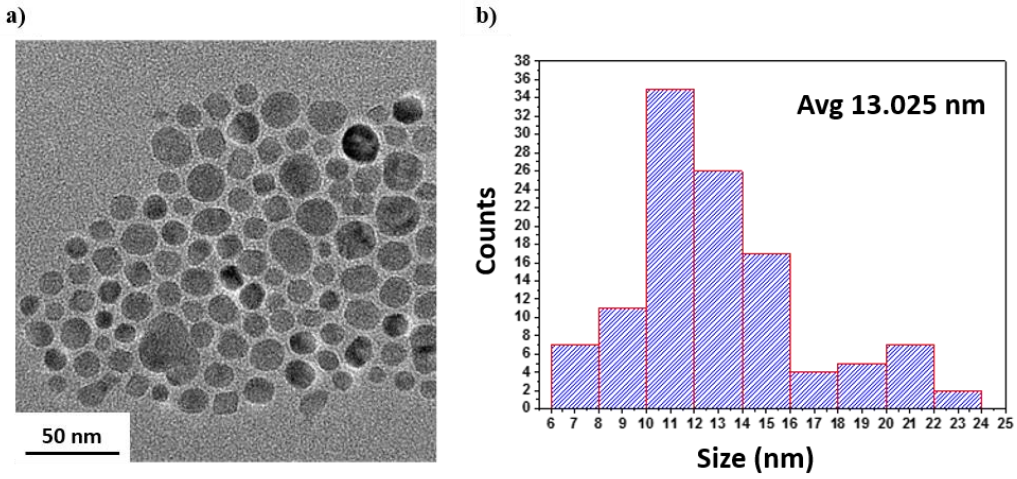

Fig. 2.4. a) TEM image and b) its size histogram of the as-synthesized 13 nm sized FeCo

nanoparticles.

On the contrary, high oleic acid makes iron and cobalt oleate complexes. So, iron and cobalt sources can be consumed for the growth of the nanoparticles, leading to increasing the size of the nanoparticles. For deeper research on surfactants, I reduced the total amount of surfactants to 1/3, leading to 5 nm FeCo nanoparticles (Figure 2.5).

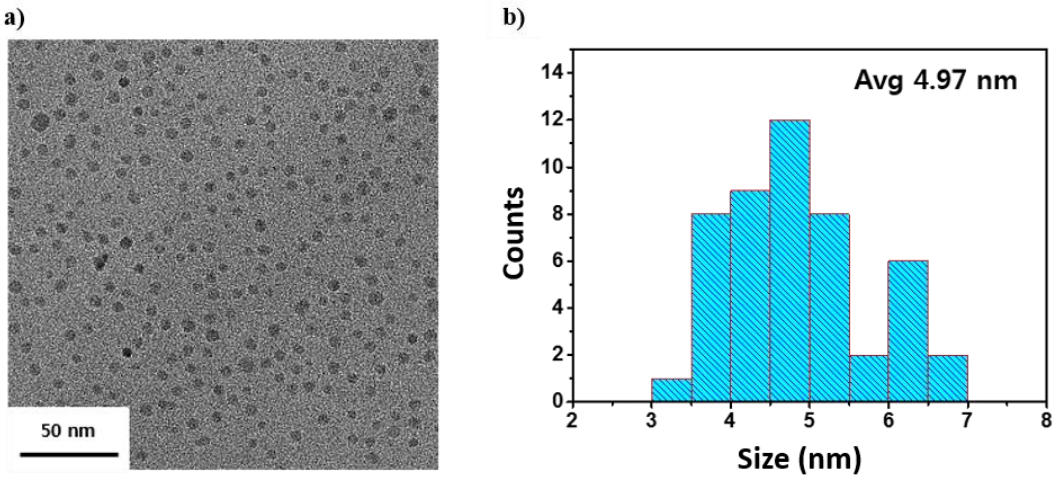

Fig. 2.5. a) TEM image and b) its size histogram of the as-synthesized 5 nm sized FeCo nanoparticles.

I observed star-shaped FeCo nanoparticles with the ratio of OA : Olam = 4 : 1 (Fig 2.6). During synthesis, OA molecules are attached to the lowest energy {100} facets and inhibit the growth of the nanoparticles in the [100] direction by forming a dense surfactant layer.[66-68] As this crystal plane is blocked, metal ions are absorbed on {111} or {110} planes. So, various shape such as star-shaped nanoparticles can be synthesized.

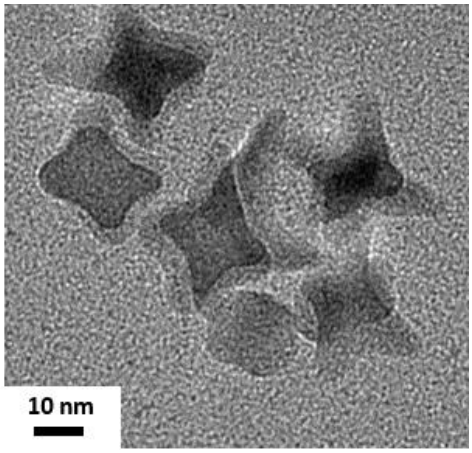

Fig. 2.6. TEM image of the star-shaped FeCo nanoparticles.

2.4 conclusion

I synthesized FeCo nanoparticles with thermal decomposition method using organometallic chemicals. Low-oxygen contained FeCo nanoparticles are formed as hydrogen gas directly injected in the reaction mixture. Various size and shape of FeCo nanoparticles were also synthesized varying the amount and ratio of oleic acid and oleylamine. A various range of applications such bio-application, data storage, electromagnetic wave shielding, biomedical products would be more developed with the various FeCo nanoparticles.

Chapter 3. Attachment magnetic nanoparticles to edge-oxidized graphene

3.1 Introduction

Graphene, which is an allotrope of carbon, has structure of a plane sp^2 bonded atom.[69-71] It has large surface area, superior thermal, electrical and mechanical properties.[72-75] Attachment nanoparticles on graphene has also attracted considerable interest because the composites have great potential for a wide variety of application such as catalyst, optoelectronic materials, sensors.[76-80] Among nanoparticles/graphene composites, magnetic nanoparticle and graphene oxide composite are promising because they can be used in a sensor, drug delivery, magnetic resonance imaging, anode of Li-ion batteries, and electromagnetic wave absorption shielding.[82-85] There are many researches about attachment magnetic nanoparticles on graphene using graphene oxide.[86] The main advantages of using graphene oxide is that it is easy to disperse in water or other solvent since it has carboxylic acid and hydroxylic functionalities. In this respect, there have been many methods of synthesizing magnetic nanoparticles and graphene oxide. Szabo et al.[87] synthesized iron oxide nanoparticles and graphene hybrids from using tris(2,2'-bipyridyl) iron(II) ion and graphene oxide through ion exchange. Also, Cong et al.[83] prepared magnetic nanoparticles decorated graphene oxide through a high temperature decomposition method, which can be used in magnetic resonance imaging. But in-situ method of synthesizing magnetic nanoparticles and graphene has some problems because it is hard to control the size of nanoparticles and location of magnetic nanoparticles on the graphene oxide. To overcome these drawbacks, Zhang et al.[88] discovered ex-situ method of synthesizing the composites. At first, they synthesized monodisperse Fe_3O_4 nanoparticles and introduce 2,3-dimercaptosuccinnic acid (DMSA) to the nanoparticles. And graphene oxide is reduced and functionalized by polyethyleneimine(PEI) by simply heating the PEI and graphene oxide mixture at 60°C for 12 hours. DMSA modified Fe3O4 nanoparticles can be easily attached on PEI-GO by EDC coupling method.

In this paper, I synthesized magnetic nanoparticles and edge-oxidized graphene(EOG) composite. EOG has carboxylic acid and hydroxyl functionalities only at the edge of it.[89] So, it has great dispensability on water and better electrical properties than graphene oxide. I synthesized the composite using two methods; (1) EDC coupling which is mentioned above, and (2) using electrostatic interaction. In second method, the surface of FeCo nanoparticles are exchanged organic ligands into inorganic ligand to change the charge of nanoparticles to (-), while PEI-coated graphene oxide has charge of (+). I synthesized FeCo nanoparticles and EOG hybrid materials through electrostatic interaction.

3.2 experimental method

Chemicals

Iron (III) acetylacetonate ($Fe(acac)_3$, 99.9 %, Sigma-Aldrich), cobalt (II) acetylacetonate ($Co(acac)_2$, 97 %, Sigma-Aldrich), 1,2-hexadecanediol (90 %, Sigma-Aldrich), oleic acid (OA, 90 %, Sigma-Aldrich), oleylamine (Olam, 70 %, Sigma-Aldrich), dibenzyl ether (98 %, Sigma-Aldrich), ammonium chloride (NH_4Cl, 99.5 %, Samchun chemical), polyethyleneimine (PEI, average M_w ~25,000 by LS, average M_n ~10,000 by GPC, branched). Edge-oxidized graphene (EOG) was supplied from Mexplroer Co., Ltd.

Characterization

Transmission electron microscopy (TEM) images of nanocrystals (NCs) were obtained using a JEOL-2100 instrument operated at 200 kV. The optical absorption of NCs were acquired at room temperature using a Cary 5000 UV-Vis-NIR spectrophotometer. ζ- potential data were collected using a Malvern Zetasizer Nano-ZS.

Synthesis of $CoFe_2O_4$ nanoparticles,

All reactions were carried out using Schlenk line technique. At first, $Fe(acac)_3$ (0.3680 g, 1 mmol), $Co(acac)_2$ (0.5355 g, 2 mmol), 1,2-hexadecandiol (0.9675 g, 3 mmol) and dibenzyl ether (50.0 mL) were mixed in a reaction flask. The reaction solvent was degassed for 30 minutes using nitrogen gas to allow the removal of air. And temperature of the mixture was raised to 100°C and maintain this temperature for 10 minutes. Then, OA (4 mL) and Olam (4.25 mL) were added in the 50 mL flask. The mixture was heated to 200°C for 20 minutes. Finally, the mixture is heated to 300°C for 60 minutes with reflux. After cooling it to 25°C, 5 mL of hexane was injected in the flask. The synthesized $CoFe_2O_4$ nanoparticles were precipitated by the addition of 15 mL of ethanol and centrifugation (6000 rpm, 5 minutes) and re-dispersed in hexane. The washing process were done several times to remove the residual of the resultant. Final product was dispersed in 10 mL of hexane.

Modification of the $CoFe_2O_4$ nanoparticles by DMSA

40 mg of the as-synthesized $CoFe_2O_4$ nanoparticles was dissolved in 4 mL toluene followed by addition of a solution containing 40 mg DMSA and 4 mL DMSO. The mixture solution was stirred at room temperature for 12 hours. And the resultant was washed with distilled water by magnetic separation three times. DMSA modified $CoFe_2O_4$ nanoparticles are finally dispersed in distilled water.

PEI coating of edge-oxidized graphene

5mg of edge-oxidized graphene and 50 mL PEI (1 vol%) were mixed in 200 mL flask. And temperature of the reaction mixture was raised to 60°C and maintain this temperature for 12 hours. After cooling to 25°C, the mixture was precipitated by centrifugation (7830 rpm, 20 minutes). The washing process was repeated for three times and re-dispersed in 10 mL of DI water (0.5 mg/mL).

Formation of $CoFe_2O_4$/EOG composites

The mixture of 40 mg of $CoFe_2O_4$ nanoparticles and 5 mg of PEI-EOG, 80 mg of EDC, 80 mg of NHS was stirred at 25°C for 2 days. The composite was centrifuged, then repeated 3 times for washing to eliminate residual.

Ligand exchange of FeCo nanoparticles with Cl^- ligands and formation of FeCo/EOG composites

40 mg of FeCo nanoparticles (4 mg/mL) was added to a vial containing 200 mg of NH_4Cl dissolved in 10 mL of DI water. The immiscible two-phase mixture was stirred vigorously until the phase transfer of FeCo nanoparticles from the upper hexane phase to bottom DI water phase is completed. It usually takes 3 days to complete the ligand exchange. After ligand exchange, upper hexane phase was discarded and then collected bottom solution was precipitated by the addition of 40 mL of isopropanol (IPA). This washing process was repeated three times to remove the unreacted Cl^- ligands completely and Cl-capped FeCo nanoparticles were re-dispersed in 10 mL of DI water. To attach Cl^- capped FeCo nanoparticles to edge-oxidized graphene, the nanoparticles and EOG were mixed with the ratio of 8 : 1.

3.3 Result and discussion

3.3.1 Attachment cobalt ferrite nanoparticles to EOG by EDC coupling

1-Ethyl-3-(3-dimethylaminopropyl)-carbodiimide (EDC) is a zero-length crosslinking agent used to couple carboxyl groups to amine groups. One of the advantages of EDC coupling is that the reaction can be done in water, which allows the reaction without the aids of organic solvent. However, the coupling reaction must be carried out fast, as the reactive ester can be rapidly hydrolyzed. So, N-hydroxysuccinimide (NHS) is needed for stability of the reaction. pH, the amount of EDC and the ratio of EDC/NHS which are the key parameters of EDC coupling should be well controlled not to aggregate due to loss of electrostatic repulsive forces among NPs. In this paper, attachment cobalt ferrite nanoparticles to edge-oxidized graphene was carried out by the EDC coupling (Figure 3.1).

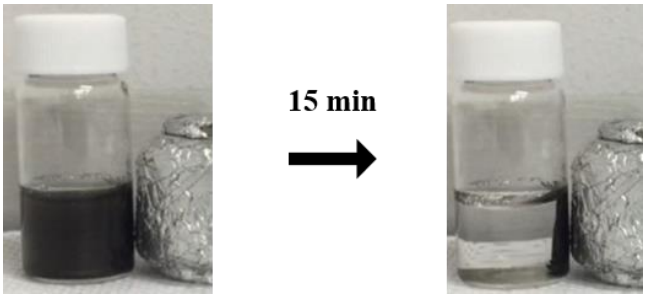

Fig. 3.1 $CoFe_2O_4$/EOG composites in water and its magnetic property

The scheme of synthesizing the composites is illustrated in Figure 3.2. At first, cobalt ferrite ($CoFe_2O_4$) nanoparticles are synthesized by thermal-decomposition method. Then, 2,3-dimercaptosuccinnic acid (DMSA) was introduced to the surface of the nanoparticles. There are two reasons of choosing DMSA. One reason is to introduce carboxylic group (-COOH) needed for EDC coupling. The other reason is that DMSA coated nanoparticles can be dissolved into water due to carboxylic group.

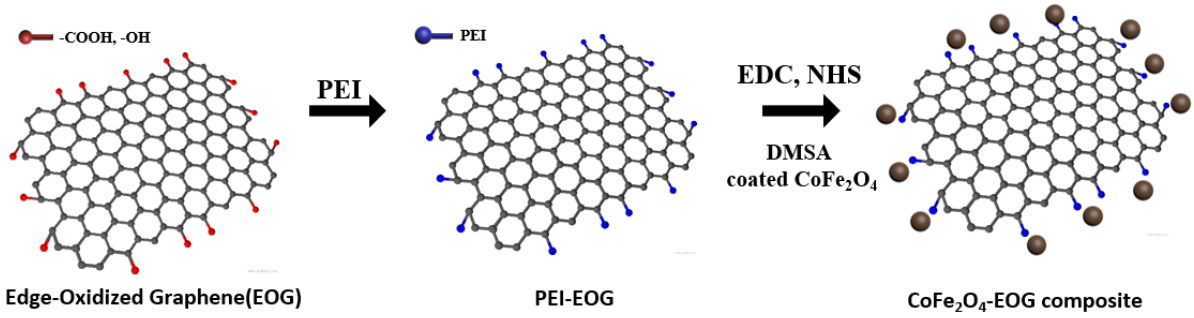

Fig. 3.2. Illustration of the fabrication of $CoFe_2O_4$/EOG composite by EDC coupling method.

Edge-oxidized graphene (EOG) was coated with polyethyleneimine (PEI) for EDC coupling. The amine group ($-NH_2$) of PEI is essential for EDC coupling. At first, 50 mL of EOG (0.1 mg/mL) are added to 1% of 50 mL PEI. The mixture was heated to 60°C for 12 hours. As a result, the functionalities of EOG was reduced because of amine group in PEI. The PEI-EOG was characterized by UV-vis, Raman and zeta-potential. There are observable shift of characteristic peaks from 265 to 272 nm in the UV-vis spectra. This shift suggests reduction of EOG and restoration of the large electronic conjugation (figure 3.3a). [90-91] As can be seen in Raman spectra, peaks of D band were shifted from 1351 cm^{-1} to 1343 cm^{-1} and peaks of G band were shifted from 1590 cm^{-1} to 1585 cm^{-1}.[92-93] The shift is also typical features of reduction of graphene oxide. The zeta potential of PEI-EOG had positive value, while zeta potential of original EOG couldn't be measured. This indicates positive charge was induced to PEI-EOG complex (Figure 3.7).

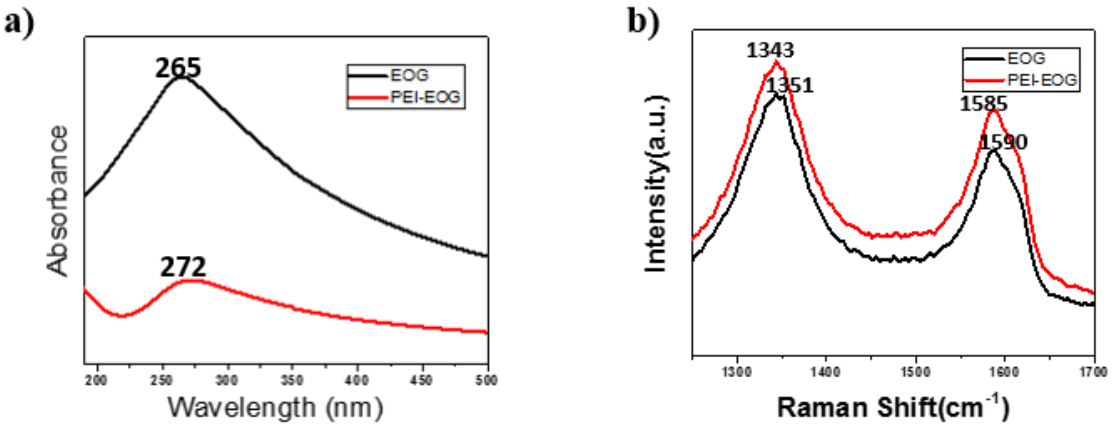

Fig. 3.3. a) Absorbance spectra and b) Raman spectra of original edge-oxidized graphene and PEI coated EOG.

Formation of $CoFe_2O_4$ and EOG composites was carried out by EDC coupling. EDC and NHS are added to the mixture of PEI-EOG and DMSA-coated $CoFe_2O_4$ nanoparticles for chemical bonding of the composites. The $CoFe_2O_4$/EOG composites were characterized by transmission electron microscope. Figure 3.4 shows TEM image of $CoFe_2O_4$/EOG composites by EDC coupling. The $CoFe_2O_4$ nanoparticles were attached to the edge of the EOG, suggesting that PEI was introduced to edge part of EOG.

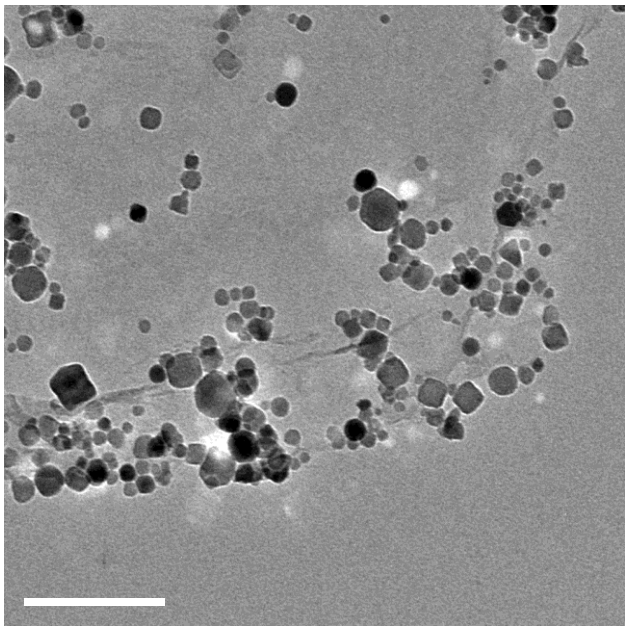

Fig. 3.4. TEM image of the $CoFe_2O_4$-EOG composites by EDC coupling.

3.3.2 Attachment FeCo nanoparticles to EOG by electrostatic interaction

Most routes for synthesizing nanoparticles include long hydrocarbon chain organic ligands. They play a key role in the formation of nanoparticles, and stabilize the nanoparticles by prevent agglomeration.[94] However, it is hard to use nanoparticles capped with organic ligands as electrical device or catalyst, because long-chain ligands are acting as an electrically insulating barrier for charge transport, blocking the access of other species. Recently, there are many reports about exchanging organic ligands with inorganic ligands such as $In_2Se_4^{2-}$, MoS_4^{2-}, Cl^- and so on. Inorganic ligands remarkably improve the charge transport properties of nanoparticles because of strong electronic coupling arising from shorter interparticle distance.[95-98] Typically, nanoparticles capped with organic ligands dissolve in organic solvent like hexane and toluene, because steric stabilization is dominant mechanism of dispersion. On the contrary, nanoparticles capped with inorganic ligands dissolve in polar solvent such as water, because electrostatic stabilization is the main mechanism of dispersion.

Unlike $CoFe_2O_4$ nanoparticles, it is hard to adjust DMSA to the surface of FeCo nanoparticles. I assumed that the lack of boding sites results in the problem. For this reason, there should be another method for formation of FeCo/EOG. In this paper, I suggest using electrostatic interaction can be the answer. The scheme of the formation of FeCo/EOG composites are illustrated in figure 3.5.

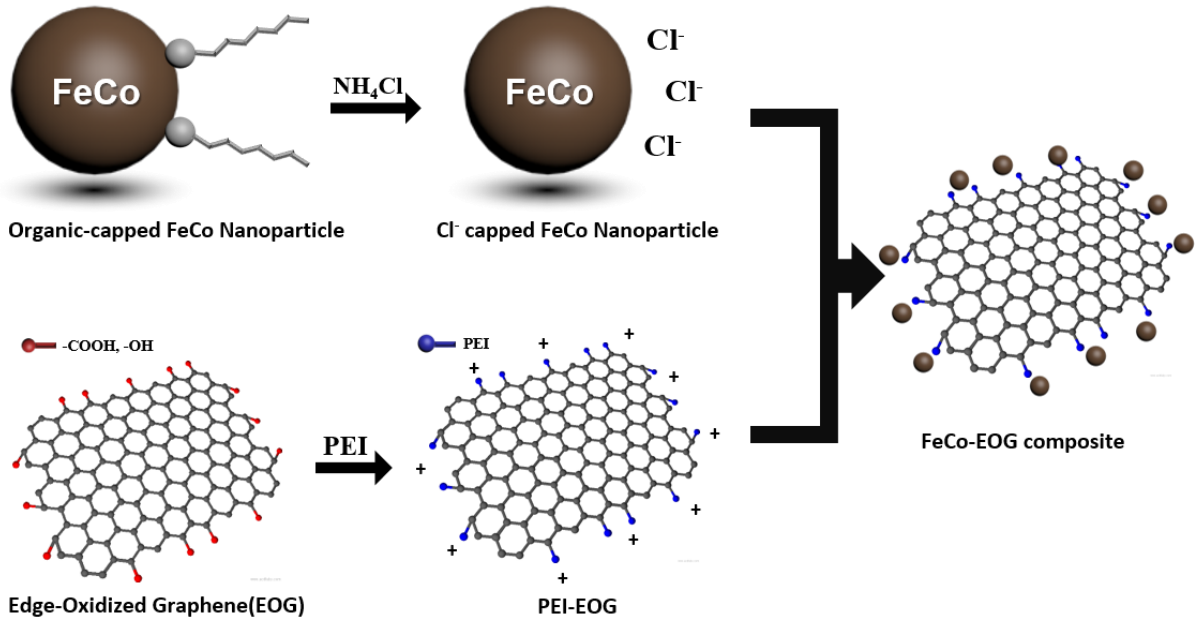

Fig. 3.5. Illustration of the fabrication of FeCo/EOG composite by electrostatic interaction.

At first, I introduced inorganic ligands to the surface of FeCo nanoparticles (figure 3.6). There are two

reasons about using inorganic ligands for formation of FeCo/EOG composites. First, inorganic ligand capped FeCo can be dissolved in water by electrostatic stabilization. The other reason is to introduce negative surface charge. The inorganic ligands (Cl^-) capped FeCo nanoparticles were characterized by TEM and zeta-potential.

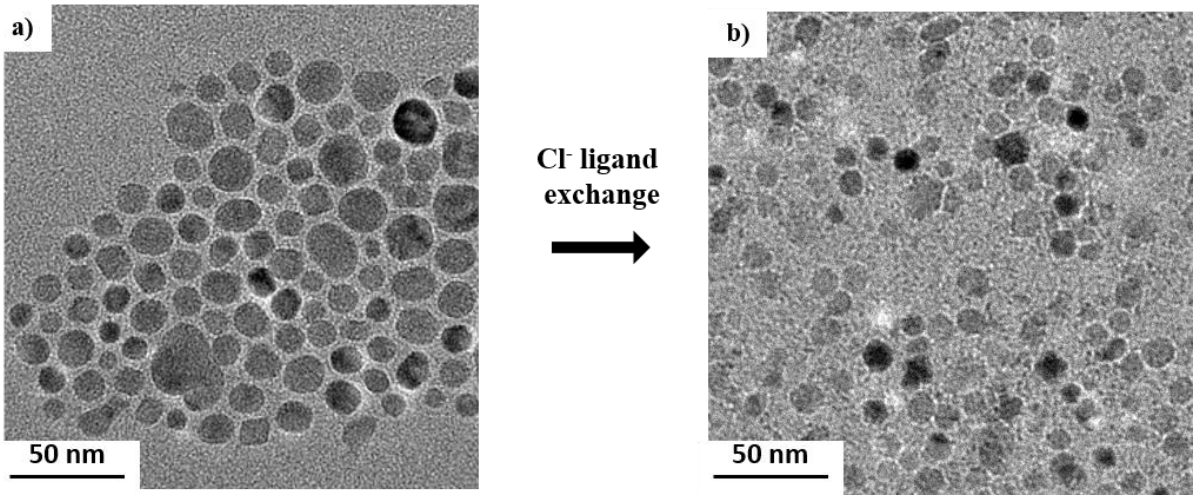

Fig. 3.6. TEM images of a) as-synthesized FeCo nanoparticles and b) Cl^- capped FeCo nanoparticles

Figure 3.7 shows TEM images of Cl^- capped FeCo nanoparticles, suggesting that the shape or size of the nanoparticles was unchanged. The zeta potential of Cl^- capped FeCo had negative value, while the zeta potential of PEI-EOG had positive value.

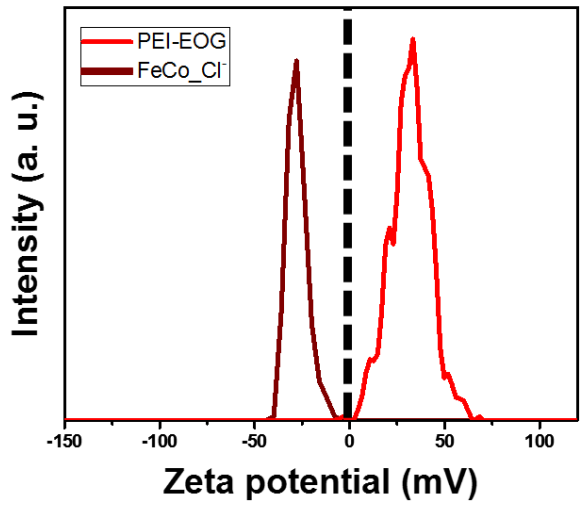

Fig. 3.7. Zeta potential of PEI coated edge-oxidized graphene and Cl^- capped FeCo

For the formation of FeCo/EOG composite, I just mixed Cl^- capped FeCo and PEI-EOG in water. After stirring all night long, the FeCo/EOG composite are characterized by TEM. Figure 3.8 shows TEM images of FeCo/EOG composites. The FeCo nanoparticles were attached to the edge of the EOG, suggesting of the formation of the composites.

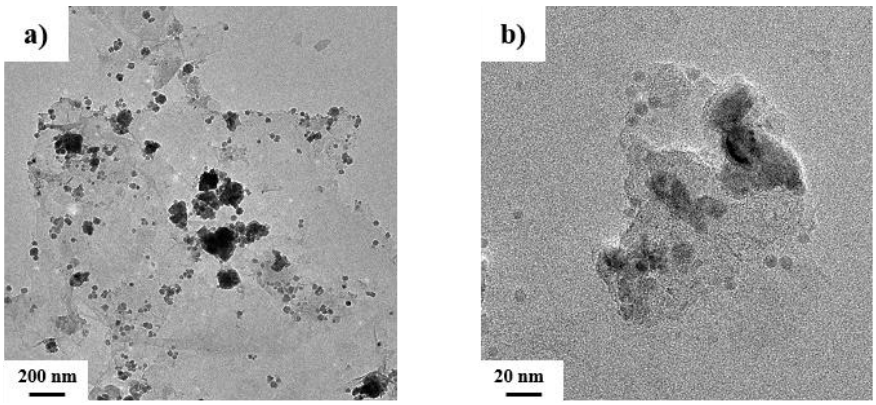

Fig. 3.8. TEM images of a) 13-nm FeCo and EOG composites and b) 5-nm FeCo and EOG composite.

3.4 Conclusion

In conclusion, the attachment of magnetic nanoparticles to edge-oxidized graphene was done with two different methods. First, I made PEI coated EOG and checked them with UV-vis, Raman and zeta potential. $CoFe_2O_4$ nanoparticles and PEI-EOG composites were formed with EDC coupling chemistry. Cl^- nanoparticles and PEI-EOG were attached to each other by electrostatic interaction. The MNP/EOG composites are expected to use in various range of application such as bio-sensors, lithium ion secondary battery, electromagnetic wave absorption and biomedical application.

References

1. Volokitin, Y.; Sinzig, J.; de Jongh, L. J.; Schmid, G.; Vargaftik, M. N.; Moiseevi, I. I., Quantum-size effects in the thermodynamic properties of metallic nanoparticles. *Nature* **1996,** *384* (6610), 621-623.
2. Chin, S. F.; Iyer, K. S.; Raston, C. L.; Saunders, M., Size Selective Synthesis of Superparamagnetic Nanoparticles in Thin Fluids under Continuous Flow Conditions. *Advanced Functional Materials* **2008,** *18* (6), 922-927.
3. Wang, F.; Dong, A.; Buhro, W. E., Solution-Liquid-Solid Synthesis, Properties, and Applications of One-Dimensional Colloidal Semiconductor Nanorods and Nanowires. *Chem Rev* **2016,** *116* (18), 10888-933.
4. Taylor, R.; Coulombe, S.; Otanicar, T.; Phelan, P.; Gunawan, A.; Lv, W.; Rosengarten, G.; Prasher, R.; Tyagi, H., Small particles, big impacts: A review of the diverse applications of nanofluids. *Journal of Applied Physics* **2013,** *113* (1), 011301.
5. Hewakuruppu, Y. L.; Dombrovsky, L. A.; Chen, C.; Timchenko, V.; Jiang, X.; Baek, S.; Taylor, R. A., Plasmonic "pump-probe" method to study semi-transparent nanofluids. *Appl Opt* **2013,** *52* (24), 6041-50.
6. Taylor, R. A.; Otanicar, T.; Rosengarten, G., Nanofluid-based optical filter optimization for PV/T systems. *Light: Science & Applications* **2012,** *1* (10), e34.
7. Gittleman, J. I.; Abeles, B.; Bozowski, S., Superparamagnetism and relaxation effects in granular Ni-SiO2and Ni-Al2O3films. *Physical Review B* **1974,** *9* (9), 3891-3897.
8. Lu, A. H.; Schmidt, W.; Matoussevitch, N.; Bonnemann, H.; Spliethoff, B.; Tesche, B.; Bill, E.; Kiefer, W.; Schuth, F., Nanoengineering of a magnetically separable hydrogenation catalyst. *Angew Chem Int Ed Engl* **2004,** *43* (33), 4303-6.
9. Ramaswamy, B.; Kulkarni, S. D.; Villar, P. S.; Smith, R. S.; Eberly, C.; Araneda, R. C.; Depireux, D. A.; Shapiro, B., Movement of magnetic nanoparticles in brain tissue: mechanisms and impact on normal neuronal function. *Nanomedicine* **2015,** *11* (7), 1821-9.
10. Mornet, S.; Vasseur, S.; Grasset, F.; Veverka, P.; Goglio, G.; Demourgues, A.; Portier, J.; Pollert, E.; Duguet, E., Magnetic nanoparticle design for medical applications. *Progress in Solid State Chemistry* **2006,** *34* (2-4), 237-247.
11. Hyeon, T., Chemical synthesis of magnetic nanoparticles. *Chemical Communications* **2003,** (8), 927-934.
12. Chen, Y. J.; Gao, P.; Zhu, C. L.; Wang, R. X.; Wang, L. J.; Cao, M. S.; Fang, X. Y., Synthesis, magnetic and electromagnetic wave absorption properties of porous Fe3O4/Fe/SiO2 core/shell nanorods. *Journal of Applied Physics* **2009,** *106* (5), 054303.

13. Arruebo, M.; Fernández-Pacheco, R.; Ibarra, M. R.; Santamaría, J., Magnetic nanoparticles for drug delivery. *Nano Today* **2007,** *2* (3), 22-32.
14. Sun, S., Monodisperse FePt Nanoparticles and Ferromagnetic FePt Nanocrystal Superlattices. *Science* **2000,** *287* (5460), 1989-1992.
15. Sun, S.; Zeng, H.; Robinson, D. B.; Raoux, S.; Rice, P. M.; Wang, S. X.; Li, G., Monodisperse MFe2O4 (M = Fe, Co, Mn) nanoparticles. *J Am Chem Soc* **2004,** *126* (1), 273-9.
16. Gu, H.; Zheng, R.; Zhang, X.; Xu, B., Facile one-pot synthesis of bifunctional heterodimers of nanoparticles: a conjugate of quantum dot and magnetic nanoparticles. *J Am Chem Soc* **2004,** *126* (18), 5664-5.
17. Bulte, J. W.; Kraitchman, D. L., Iron oxide MR contrast agents for molecular and cellular imaging. *NMR Biomed* **2004,** *17*(7), 484-99.
18. Huber, D. L., Synthesis, properties, and applications of iron nanoparticles. *Small* **2005,** *1* (5), 482-501.
19. Wu, L.; Li, Q.; Wu, C. H.; Zhu, H.; Mendoza-Garcia, A.; Shen, B.; Guo, J.; Sun, S., Stable Cobalt Nanoparticles and Their Monolayer Array as an Efficient Electrocatalyst for Oxygen Evolution Reaction. *J Am Chem Soc* **2015,** *137* (22), 7071-4.
20. Han, M. J.; Ozaki, T.; Yu, J., Electronic structure and magnetic properties of small manganese oxide clusters. *J Chem Phys* **2005,** *123* (3), 34306.
21. Assadi, M. H. N.; Hanaor, D. A. H., Theoretical study on copper's energetics and magnetism in TiO2 polymorphs. *Journal of Applied Physics* **2013,** *113* (23), 233913.
22. Batlle, X.; Labarta, A., Finite-size effects in fine particles: magnetic and transport properties. *Journal of Physics D: Applied Physics* **2002,** *35* (6), R15-R42.
23. Leslie-Pelecky, D. L.; Rieke, R. D., Magnetic Properties of Nanostructured Materials. *Chemistry of Materials* **1996,** *8* (8), 1770-1783.
24. Iwaki, T.; Kakihara, Y.; Toda, T.; Abdullah, M.; Okuyama, K., Preparation of high coercivity magnetic FePt nanoparticles by liquid process. *Journal of Applied Physics* **2003,** *94* (10), 6807-6811.
25. Soumare, Y.; Garcia, C.; Maurer, T.; Chaboussant, G.; Ott, F.; Fiévet, F.; Piquemal, J.-Y.; Viau, G., Kinetically Controlled Synthesis of Hexagonally Close-Packed Cobalt Nanorods with High Magnetic Coercivity. *Advanced Functional Materials* **2009,** *19* (12), 1971-1977.
26. Sun, S., Recent Advances in Chemical Synthesis, Self-Assembly, and Applications of FePt Nanoparticles. *Advanced Materials* **2006,** *18* (4), 393-403.
27. Laughlin, D. E.; Srinivasan, K.; Tanase, M.; Wang, L., Crystallographic aspects of L10 magnetic materials. *Scripta Materialia* **2005,** *53* (4), 383-388.
28. de la Pena O'Shea, V. A.; Moreira Ide, P.; Roldan, A.; Illas, F., Electronic and magnetic structure

of bulk cobalt: the alpha, beta, and epsilon-phases from density functional theory calculations. *J Chem Phys* **2010,** *133* (2), 024701.

29. Respaud, M.; Broto, J. M.; Rakoto, H.; Fert, A. R.; Thomas, L.; Barbara, B.; Verelst, M.; Snoeck, E.; Lecante, P.; Mosset, A.; Osuna, J.; Ely, T. O.; Amiens, C.; Chaudret, B., Surface effects on the magnetic properties of ultrafine cobalt particles. *Physical Review B* **1998,** *57* (5), 2925-2935.
30. Bodker, F.; Morup, S.; Linderoth, S., Surface effects in metallic iron nanoparticles. *Phys Rev Lett* **1994,** *72* (2), 282-285.
31. Lee, J. H.; Huh, Y. M.; Jun, Y. W.; Seo, J. W.; Jang, J. T.; Song, H. T.; Kim, S.; Cho, E. J.; Yoon, H. G.; Suh, J. S.; Cheon, J., Artificially engineered magnetic nanoparticles for ultra-sensitive molecular imaging. *Nat Med* **2007,** *13* (1), 95-9.
32. Shouheng, S.; Fullerton, E. E.; Weller, D.; Murray, C. B., Compositionally controlled FePt nanoparticle materials. *IEEE Transactions on Magnetics* **2001,** *37* (4), 1239-1243.
33. Gutfleisch, O.; Lyubina, J.; Müller, K. H.; Schultz, L., FePt Hard Magnets. *Advanced Engineering Materials* **2005,** *7* (4), 208-212.
34. LaMer, V. K.; Dinegar, R. H., Theory, Production and Mechanism of Formation of Monodispersed Hydrosols. *Journal of the American Chemical Society* **1950,** *72* (11), 4847-4854.
35. Erdemir, D.; Lee, A. Y.; Myerson, A. S., Nucleation of crystals from solution: classical and two-step models. *Acc Chem Res* **2009,** *42* (5), 621-9.
36. Murray, C. B.; Norris, D. J.; Bawendi, M. G., Synthesis and characterization of nearly monodisperse CdE (E = sulfur, selenium, tellurium) semiconductor nanocrystallites. *Journal of the American Chemical Society* **1993,** *115* (19), 8706-8715.
37. Peng, S.; Wang, C.; Xie, J.; Sun, S., Synthesis and stabilization of monodisperse Fe nanoparticles. *J Am Chem Soc* **2006,***128* (33), 10676-7.
38. Lacroix, L. M.; Huls, N. F.; Ho, D.; Sun, X.; Cheng, K.; Sun, S., Stable single-crystalline body centered cubic Fe nanoparticles. *Nano Lett* **2011,** *11* (4), 1641-5.
39. Puntes, V. F.; Zanchet, D.; Erdonmez, C. K.; Alivisatos, A. P., Synthesis of hcp-Co Nanodisks. *Journal of the American Chemical Society* **2002,** *124* (43), 12874-12880.
40. Black, C. T., Spin-Dependent Tunneling in Self-Assembled Cobalt-Nanocrystal Superlattices. *Science* **2000,** *290* (5494), 1131-1134.
41. Park, J.; Kang, E.; Son, S. U.; Park, H. M.; Lee, M. K.; Kim, J.; Kim, K. W.; Noh, H. J.; Park, J. H.; Bae, C. J.; Park, J. G.; Hyeon, T., Monodisperse Nanoparticles of Ni and NiO: Synthesis, Characterization, Self-Assembled Superlattices, and Catalytic Applications in the Suzuki Coupling Reaction. *Advanced Materials* **2005,** *17* (4), 429-434.
42. Sun, S.; Zeng, H., Size-Controlled Synthesis of Magnetite Nanoparticles. *Journal of the American Chemical Society* **2002,***124* (28), 8204-8205.

43. Park, J.; An, K.; Hwang, Y.; Park, J. G.; Noh, H. J.; Kim, J. Y.; Park, J. H.; Hwang, N. M.; Hyeon, T., Ultra-large-scale syntheses of monodisperse nanocrystals. *Nat Mater* **2004,** *3* (12), 891-5.
44. Lopez-Lopez, M. T.; Duran, J. D.; Delgado, A. V.; Gonzalez-Caballero, F., Stability and magnetic characterization of oleate-covered magnetite ferrofluids in different nonpolar carriers. *J Colloid Interface Sci* **2005,** *291* (1), 144-51.
45. Viota, J. L.; Durán, J. D. G.; González-Caballero, F.; Delgado, A. V., Magnetic properties of extremely bimodal magnetite suspensions. *Journal of Magnetism and Magnetic Materials* **2007,** *314* (2), 80-86.
46. Massart, R., Preparation of aqueous magnetic liquids in alkaline and acidic media. *IEEE Transactions on Magnetics* **1981,***17* (2), 1247-1248.
47. Khollam, Y. B.; Dhage, S. R.; Potdar, H. S.; Deshpande, S. B.; Bakare, P. P.; Kulkarni, S. D.; Date, S. K., Microwave hydrothermal preparation of submicron-sized spherical magnetite (Fe3O4) powders. *Materials Letters* **2002,** *56* (4), 571-577.
48. Chen, F.; Gao, Q.; Hong, G.; Ni, J., Synthesis and characterization of magnetite dodecahedron nanostructure by hydrothermal method. *Journal of Magnetism and Magnetic Materials* **2008,** *320* (11), 1775-1780.
49. Ge, S.; Shi, X.; Sun, K.; Li, C.; Baker, J. R.; Banaszak Holl, M. M.; Orr, B. G., A Facile Hydrothermal Synthesis of Iron Oxide Nanoparticles with Tunable Magnetic Properties. *J Phys Chem C Nanomater Interfaces* **2009,** *113* (31), 13593-13599.
50. Jasieniak, J.; Bullen, C.; van Embden, J.; Mulvaney, P., Phosphine-free synthesis of CdSe nanocrystals. *J Phys Chem B* **2005,***109* (44), 20665-8.
51. Liu, C.; Zou, B.; Rondinone, A. J.; Zhang, Z. J., Reverse Micelle Synthesis and Characterization of Superparamagnetic MnFe2O4Spinel Ferrite Nanocrystallites. *The Journal of Physical Chemistry B* **2000,** *104* (6), 1141-1145.
52. Lu, A. H.; Salabas, E. L.; Schuth, F., Magnetic nanoparticles: synthesis, protection, functionalization, and application. *Angew Chem Int Ed Engl* **2007,** *46* (8), 1222-44.
53. Yang, H.; Zhang, J.; Tian, Q.; Hu, H.; Fang, Y.; Wu, H.; Yang, S., One-pot synthesis of amphiphilic superparamagnetic FePt nanoparticles and magnetic resonance imaging in vitro. *Journal of Magnetism and Magnetic Materials* **2010**, 322 (8), 973-977.
54. Feng, Y.; Qiu, T., Preparation, characterization and microwave absorbing properties of FeNi alloy prepared by gas atomization method. *Journal of Alloys and Compounds* **2012**, 513, 455-459.
55. Rafique, M. Y.; Pan, L.; Zubair Iqbal, M.; Javed, Q.-u.-a.; Qiu, H.; Rafi ud, d.; Farooq, M. H.; Guo, Z., 3-D flower like FeCo alloy nanostructures assembled with nanotriangular prism: Facile synthesis, magnetic properties, and effect of NaOH on its formation. *Journal of Alloys and*

Compounds **2013**, 550, 423-430.

56. Lacroix, L. M.; Malaki, R. B.; Carrey, J.; Lachaize, S.; Respaud, M.; Goya, G. F.; Chaudret, B., Magnetic hyperthermia in single-domain monodisperse FeCo nanoparticles: Evidences for Stoner–Wohlfarth behavior and large losses. *Journal of Applied Physics* **2009**, 105 (2), 023911.
57. Kodama, D.; Shinoda, K.; Sato, K.; Konno, Y.; Joseyphus, R. J.; Motomiya, K.; Takahashi, H.; Matsumoto, T.; Sato, Y.; Tohji, K.; Jeyadevan, B., Chemical Synthesis of Sub-micrometer- to Nanometer-Sized Magnetic FeCo Dice. *Advanced Materials* **2006**, 18 (23), 3154-3159.
58. Chaubey, G. S.; Barcena, C.; Poudyal, N.; Rong, C.; Gao, J.; Sun, S.; Liu, J. P., Synthesis and stabilization of FeCo nanoparticles. *J Am Chem Soc* **2007**, 129 (23), 7214-5.
59. Shin, S. J.; Kim, Y. H.; Kim, C. W.; Cha, H. G.; Kim, Y. J.; Kang, Y. S., Preparation of magnetic FeCo nanoparticles by coprecipitation route. *Current Applied Physics* **2007**, 7 (4), 404-408.
60. Wei, X.-W.; Zhu, G.-X.; Liu, Y.-J.; Ni, Y.-H.; Song, Y.; Xu, Z., Large-Scale Controlled Synthesis of FeCo Nanocubes and Microcages by Wet Chemistry. *Chemistry of Materials* **2008**, 20 (19), 6248-6253.
61. Poudyal, N.; Chaubey, G. S.; Rong, C. B.; Cui, J.; Liu, J. P., Synthesis of monodisperse FeCo nanoparticles by reductive salt-matrix annealing. *Nanotechnology* **2013**, 24 (34), 345605.
62. Ung, D.; Tung, L. D.; Caruntu, G.; Delaportas, D.; Alexandrou, I.; Prior, I. A.; Thanh, N. T. K., Variant shape growth of nanoparticles of metallic Fe–Pt, Fe–Pd and Fe–Pt–Pd alloys. *CrystEngComm* **2009**, 11 (7), 1309.
63. Chen, M.; Kim, J.; Liu, J. P.; Fan, H.; Sun, S., Synthesis of FePt nanocubes and their oriented self-assembly. *J Am Chem Soc* **2006**, 128 (22), 7132-3.
64. Zhang, J.; Fang, J., A general strategy for preparation of Pt 3d-transition metal (Co, Fe, Ni) nanocubes. *J Am Chem Soc* **2009**, 131 (51), 18543-7.
65. Yang, H.; Ogawa, T.; Hasegawa, D.; Takahashi, M., Synthesis and magnetic properties of monodisperse magnetite nanocubes. *Journal of Applied Physics* **2008**, 103 (7), 07D526.
66. Song, Q.; Zhang, Z. J., Shape control and associated magnetic properties of spinel cobalt ferrite nanocrystals. *J Am Chem Soc* **2004,** 126 (19), 6164-8.
67. Davies, M. J.; Parker, S. C.; Watson, G. W., Atomistic simulation of the surface structure of spinel. *Journal of Materials Chemistry* **1994**, 4 (6), 813.
68. Kim, D; Lee, N.; Park, M.; Kim, B. H.; An, K.; Hyeon, T., Synthesis of uniform ferrimagnetic magnetite nanocubes. *J Am Chem Soc* **2009**, 131 (2), 454-5.
69. Novoselov, K. S.; Geim, A. K.; Morozov, S. V.; Jiang, D.; Zhang, Y.; Dubonos, S. V.; Grigorieva, I. V.; Firsov, A. A., Electric field effect in atomically thin carbon films. *Science* **2004**, 306 (5696), 666-9.
70. Katsnelson, M. I., Graphene: carbon in two dimensions. *Materials Today* **2007**, 10 (1-2), 20-27.

71. Reina, A.; Jia, X.; Ho, J.; Nezich, D.; Son, H.; Bulovic, V.; Dresselhaus, M. S.; Kong, J., Large area, few-layer graphene films on arbitrary substrates by chemical vapor deposition. *Nano Lett* **2009**, 9 (1), 30-5.
72. Chen, J. H.; Jang, C.; Xiao, S.; Ishigami, M.; Fuhrer, M. S., Intrinsic and extrinsic performance limits of graphene devices on SiO2. *Nat Nanotechnol* **2008,** 3 (4), 206-9.
73. Geim, A. K.; Kim, P., Carbon Wonderland. *Scientific American* **2008**, 298 (4), 90-97.
74. Kuzmenko, A. B.; van Heumen, E.; Carbone, F.; van der Marel, D., Universal optical conductance of graphite. *Phys Rev Lett* **2008**, 100 (11), 117401
75. Geim, A. K.; Novoselov, K. S., The rise of graphene. *Nat Mater* **2007**, 6 (3), 183-91.
76. Jasuja, K.; Linn, J.; Melton, S.; Berry, V., Microwave-Reduced Uncapped Metal Nanoparticles on Graphene: Tuning Catalytic, Electrical, and Raman Properties. *The Journal of Physical Chemistry Letters* **2010**, 1 (12), 1853-1860.
77. Si, Y.; Samulski, E. T., Exfoliated Graphene Separated by Platinum Nanoparticles. *Chemistry of Materials* **2008**, 20 (21), 6792-6797.
78. Xu, C.; Wang, X.; Zhu, J., Graphene−Metal Particle Nanocomposites. *The Journal of Physical Chemistry C* **2008**, 112 (50), 19841-19845.
79. Lim, H. N.; Huang, N. M.; Lim, S. S.; Harrison, I.; Chia, C. H., Fabrication and characterization of graphene hydrogel via hydrothermal approach as a scaffold for preliminary study of cell growth. *Int J Nanomedicine* **2011**, 6, 1817-23.
80. Kong, B. S.; Geng, J.; Jung, H. T., Layer-by-layer assembly of graphene and gold nanoparticles by vacuum filtration and spontaneous reduction of gold ions. *Chem Commun (Camb)* **2009**, (16), 2174-6.
81. Zhang, F.-J.; Liu, J.; Zhang, K.; Zhao, W.; Jang, W.-K.; Oh, W.-C., A novel and simple approach for the synthesis of Fe3O4-graphene composite. *Korean Journal of Chemical Engineering* **2012**, 29 (8), 989-993.
82. Yang, X.; Zhang, X.; Ma, Y.; Huang, Y.; Wang, Y.; Chen, Y., Superparamagnetic graphene oxide–Fe3O4 nanoparticles hybrid for controlled targeted drug carriers. *Journal of Materials Chemistry* **2009**, 19 (18), 2710.
83. Cong, H. P.; He, J. J.; Lu, Y.; Yu, S. H., Water-soluble magnetic-functionalized reduced graphene oxide sheets: in situ synthesis and magnetic resonance imaging applications. *Small* **2010**, 6 (2), 169-73.
84. He, F.; Fan, J.; Ma, D.; Zhang, L.; Leung, C.; Chan, H. L., The attachment of Fe3O4 nanoparticles to graphene oxide by covalent bonding. *Carbon* **2010**, 48 (11), 3139-3144.
85. Shen, J.; Hu, Y.; Shi, M.; Li, N.; Ma, H.; Ye, M., One Step Synthesis of Graphene Oxide−Magnetic Nanoparticle Composite. *The Journal of Physical Chemistry C* **2010**, 114 (3),

1498-1503.

86. Dreyer, D. R.; Park, S.; Bielawski, C. W.; Ruoff, R. S., The chemistry of graphene oxide. *Chem Soc Rev* **2010**, 39 (1), 228-40.
87. Szabo, T.; Bakandritsos, A.; Tzitzios, V.; Devlin, E.; Petridis, D.; Dekany, I., Magnetically modified single and turbostratic stacked graphenes from tris(2,2'-bipyridyl) iron(II) ion-exchanged graphite oxide. *J Phys Chem B* **2008,** 112 (46), 14461-9.
88. Zhang, F.-J.; Liu, J.; Zhang, K.; Zhao, W.; Jang, W.-K.; Oh, W.-C., A novel and simple approach for the synthesis of Fe3O4-graphene composite. *Korean Journal of Chemical Engineering* **2012**, 29 (8), 989-993.
89. Jeon, I. Y.; Shin, Y. R.; Sohn, G. J.; Choi, H. J.; Bae, S. Y.; Mahmood, J.; Jung, S. M.; Seo, J. M.; Kim, M. J.; Wook Chang, D.; Dai, L.; Baek, J. B., Edge-carboxylated graphene nanosheets via ball milling. *Proc Natl Acad Sci U S A* **2012**, 109 (15), 5588-93.
90. Yang, Q.; Pan, X.; Huang, F.; Li, K., Fabrication of High-Concentration and Stable Aqueous Suspensions of Graphene Nanosheets by Noncovalent Functionalization with Lignin and Cellulose Derivatives. *The Journal of Physical Chemistry C* **2010**, 114 (9), 3811-3816.
91. Zhu, C.; Guo, S.; Fang, Y.; Dong, S., Reducing sugar: new functional molecules for the green synthesis of graphene nanosheets. *ACS Nano* **2010**, 4 (4), 2429-37.
92. Chen, W.; Yan, L.; Bangal, P. R., Preparation of graphene by the rapid and mild thermal reduction of graphene oxide induced by microwaves. *Carbon* **2010**, 48 (4), 1146-1152.
93. Carozzi, S.; Nasini, M. G.; Schelotto, C.; Caviglia, P. M.; Barocci, S.; Cantaluppi, A.; Salit, M., Peritoneal dialysis fluid (PDF) C++ and 1,25(OH)2D3 modulate peritoneal macrophage (PM0) antimicrobial activity in CAPD patients. *Adv Perit Dial* **1990**, 6, 110-3.
94. Murray, C. B.; Norris, D. J.; Bawendi, M. G., Synthesis and characterization of nearly monodisperse CdE (E = sulfur, selenium, tellurium) semiconductor nanocrystallites. *Journal of the American Chemical Society* **1993**, 115 (19), 8706-8715.
95. Shanker, G. S.; Swarnkar, A.; Chatterjee, A.; Chakraborty, S.; Phukan, M.; Parveen, N.; Biswas, K.; Nag, A., Electronic grade and flexible semiconductor film employing oriented attachment of colloidal ligand-free PbS and PbSe nanocrystals at room temperature. *Nanoscale* **2015**, 7 (20), 9204-14.
96. Kadlag, K. P.; Rao, M. J.; Nag, A., Ligand-Free, Colloidal, and Luminescent Metal Sulfide Nanocrystals. *J Phys Chem Lett* **2013**, 4 (10), 1676-81.
97. Nag, A.; Zhang, H.; Janke, E.; Talapin, D. V., Inorganic Surface Ligands for Colloidal Nanomaterials. *Zeitschrift für Physikalische Chemie* **2015**, 229 (1-2).
98. Kovalenko, M. V.; Scheele, M.; Talapin, D. V., Colloidal nanocrystals with molecular metal chalcogenide surface ligands. *Science* **2009**, 324 (5933), 1417-20.

Ackknowledgement

저는 항상 제 인생이 저를 긍정적인 방향으로 이끌어가고 있다고 믿고 있습니다. NSE 연구실에서 석사과정을 밟을 수 있는 기회를 얻은 것 또한 그러한 과정 중 하나라고 믿고 있습니다. 20대 중반 그리고 후반의 학창시절 동안 힘든 일도 많았지만 NSE 실험실 분들 덕분에 포기하지 않고 끝까지 버틸 수 있었습니다. 손재성 교수님께서 학업적인 부분 뿐만 아니라 학업적이지 않는 부분에서도 인생의 선배로써 저에게 힘이 되는 조언과 격려를 많이 해 주셨습니다. 교수님께서는 무슨 일이든 이미 성공했다 라고 미리 생각을 하고 모든 일에 자신감과 확신을 가지고 행동하고 노력하라고 하셨습니다. 항상 자신감이 부족한 저였기에 그러한 사고 방식은 저에게 큰 힘이 되었습니다. 앞으로 사회에 나가 힘든 일이 많을 때 교수님의 말씀을 떠올리도록 하겠습니다. 손재성 교수님 뿐만 아니라 NSE 랩 구성원 모두 저에게 큰 힘이 되었습니다. 저에게 쓴 소리도 많이 해 주시고 현실적인 조언을 많이 해 주신 성훈이형, 석사 1년차 때 같이 룸메이트를 하였고 그 동안 저에게 정신적으로 많은 도움을 주신 승기형, 같이 논문 쓰느라 고생 많았던 형우, 동기로서 진짜 많이 의지했고 언제나 든든한 영혼의 듀오 민석이, 다툼이 많았지만 그래도 소중한 혜원이, 언제나 내 놀림 잘 받아주고 같이 장난 쳐준 승회, 형에게 항상 싹싹하게 대해주고 실험도 많이 도와줬던 다휘, 내가 하는 일을 언제나 응원해 줬고 옆에서 힘이 돼 주었던 승준이, 내 밑에서 정말로 실험 많이 도와줬고 언제나 형에게 잘 해줬던 성헌이, 그리고 앞으로 NSE 식구로 지내게 될 우용이까지 NSE 식구 여러분들 덕분에 제가 항상 저 답게 지낼 수 있었습니다. 앞으로도 석사 기간 2년이 가장 행복했던 순간들 중 하나로 기억 하게 될 것 같습니다. 2년 동안 여러분들과 지내면서 제 자신의 모자란 점 또한 많이 알게 되었고 앞으로 더욱 더 발전하는 PSM이 되도록 하겠습니다. 다들 모두 성공하고 행복하길 기원하겠습니다.

저희 랩 뿐만 아니라 많은 분들이 저의 석사 기간 동안에 도움이 되어 주셨습니다. 먼저 디펜스 심사위원을 맡아 주신 안광진 교수님, 조욱 교수님 감사합니다. 디펜스 때 주셨던 조언과 충고 잊지 않고 학교의 명예를 빛내는 인재가 되도록 하겠습니다. DGIST의 이종수 교수님과 도현이 덕분에 작년에 JPCL 학술지에 논문을 낼 수 있었습니다. 코발트철/그래핀 복합체를 연구하면서 한양대의 좌용호 교수님께서 그래핀을 제공 해 주셨고 영남대의 김기현 교수님 그리고 진우형께서 자기적 물성을 측정해 주시는 등 많은 도움을 받았습니다.

마지막으로 저를 항상 믿어 주시고 응원해주신 엄마, 아빠, 누나 가족분들께 정말로 감사드립니다. 저에게 항상 아낌없는 지원과 사랑을 주셨습니다. 이제는 가족한테 받았던 이러한 은혜를 보답하도록 하겠습니다. 엄마, 아빠, 누나 모두 사랑합니다~!!